UNIVERSITY OF CALIFORNIA, MERCED

LUBRICATION OF INTERMETALLIC NICKEL TITANIUM BEARING MATERIALS

A thesis submitted in partial satisfaction of the requirements
for the degree of Master of Science

in

Mechanical Engineering

by

Nicholas A. Walters

Committee in charge:

Professor Ashlie Martini, Chair
Professor Mehmet Z. Baykara
Professor Venkattraman Ayyaswamy

2019

The thesis of Nicholas A. Walters is approved, and is acceptable in quality and form for publication on microfilm and electronically:

Mehmet Z. Baykara	Date
Venkattraman Ayyaswamy	Date
Ashlie Martini, Chair	Date

University of California, Merced

2019

TABLE OF CONTENTS

LIST OF TABLES

LIST OF FIGURES

ACKNOWLEDGEMENTS

I would like to thank Dr. Chris DellaCorte at NASA Glenn Research Center for generously sharing the NiTi-Hf bearing balls and for research guidance in general. I would also like to thank Dr. Robert A. Erck for his expert advice and guidance in wear analysis. Most of all, I would like to thank Dr. Ashlie Martini for putting up with me, and in general for being an amazing advisor and mentor. I would also like to thank the other students in the Martini Research group who have helped and supported me in many ways. Particularly, I'd like to thank Arash Khajeh, Mohammad Vazirisereshk, Azhar Vellore, and Mickael Ades. I'd like to thank my mother, Audrie, for her support in every aspect of my life. Additionally I give a special thanks to Louise and Rachel Ghandhi for their generous and invaluable proof reading which made this thesis intelligible. Without these people I would be where I am today. This research was supported by the Merced nAnomaterials Center for Energy and Sensing (MACES) through the support of the National Aeronautics and Space Administration (NASA) grant no. NNX15AQ01.

ABSTRACT

60NiTi (60wt.% Ni, 40 wt.% Ti) is a highly resilient and corrosion resistant intermetallic alloy with hardness and elasticity properties suitable for bearing applications. However, lubrication of this material is still being explored since many commercial lubricants are designed to function through chemical and physical interactions with steel surfaces. Titanium rich alloys are known to have poor tribological performance and to be chemically aggressive toward lubricants. Since 60NiTi is a titanium rich alloy, and components made from 60NiTi will likely operate with a lubricant, it is vital to study how to properly lubricate 60NiTi contacts. The goal of this research is to characterize the performance of 60NiTi sliding contacts with different lubricants at a range of operating conditions. First, previous studies suggested castor oil as a natural lubricant for 60NiTi, and reported friction coefficients less than 0.01, i.e. superlubricity, when sliding against steel. Here, the robustness of those findings was explored by characterizing the friction coefficient as a function of contact pressure and surface roughness. It was found that friction under castor oil lubrication is highly sensitive to surface roughness, and that friction coefficients approaching the superlubricity regime are only achievable with very smooth surfaces, which may not be realistic in practical engineering applications. Second, a series of tests were performed to characterize the wear and friction of self-mated 60NiTi contacts lubricated by different greases in low sliding speed contacts. It was found that polytetrafluoroethylene (PTFE) thickened perfluoropolyether (PFPE) greases significantly reduced wear compared to the other greases tested by mitigating adhesive wear modes. These results provide valuable information to guide the selection of grease for 60NiTi contacts. Overall, this work lays the groundwork for future development of new greases and lubricants specifically designed for 60NiTi contacts.

Chapter 1

INTRODUCTION

1.1 Tribology

Tribology is the study of friction, wear, and lubrication between interacting surfaces in relative motion. The study is multidisciplinary in nature, encompassing elements from physics, chemistry, material science, and mechanical engineering. The term tribology comes from the Greek verb tribo (τρίβω) which the Liddel and Scott Greek lexicon translates as "to rub" or "to grind" [1]. The term was first coined by Peter Jost in 1966, in a report for the UK Department of Education and Science that highlighted the economic importance of utilizing basic principles of tribology [2]. The term tribology, and others bearing the prefix "tribo-", have since been widely adopted to more accurately describe a range of physical interactions and phenomena. Despite the recent development of the terminology, humans have been studying and utilizing basic principles of tribology for thousands of years. There is evidence of rudimentary bearings and practices of lubrication that predate recorded history [3]. After coining the term, Peter Jost later remarked that it was like "finally giving a name to a thousand-year-old baby" [4].

We now know that tribology plays a significant role both in our daily lives and at a global scale. Studies estimate that 20% of energy consumed globally is used just to overcome friction, and a further 3% is consumed in replacing equipment damaged by wear [5,6]. Due to the scale of this gross waste of energy, the International Energy Agency has identified the improvement of end-use efficiency of fuel and electricity as the single largest potential source of reducing CO_2 emissions. Additionally, it is estimated that correcting poor practices in tribology generally could result in savings on the order of 1–1.4% or more of the GDP for a typical modern industrial nation [5–7]. It has also been estimated that research and development of methods to reduce friction and mitigate wear can generate returns in the form of saving up to 50 times the cost of the research itself [6, 7].

Tribology still has many questions left to answer. There is still no model to predict the behavior of arbitrary sliding surfaces, and the main governing parameters are generally still not well understood [8, 9]. This lack of understanding is due to the extreme complexity of what may appear to be simple problems in tribology. However, recent developments in tools and methods show the potential to rapidly advance our understanding of tribology in the near future.

1.2 Surface Texture and Contact Mechanics

In order to study how surfaces interact, it is first important to have a good understanding of surfaces themselves. While the surface of a material may appear smooth to the eye, in practice no surface is ever perfectly flat. If you look closely through magnification, you will see that a typical surface is made up of rough, uneven features. The protrusions from the surface are called asperities. When two seemingly smooth surfaces touch, only a few asperities come into contact.

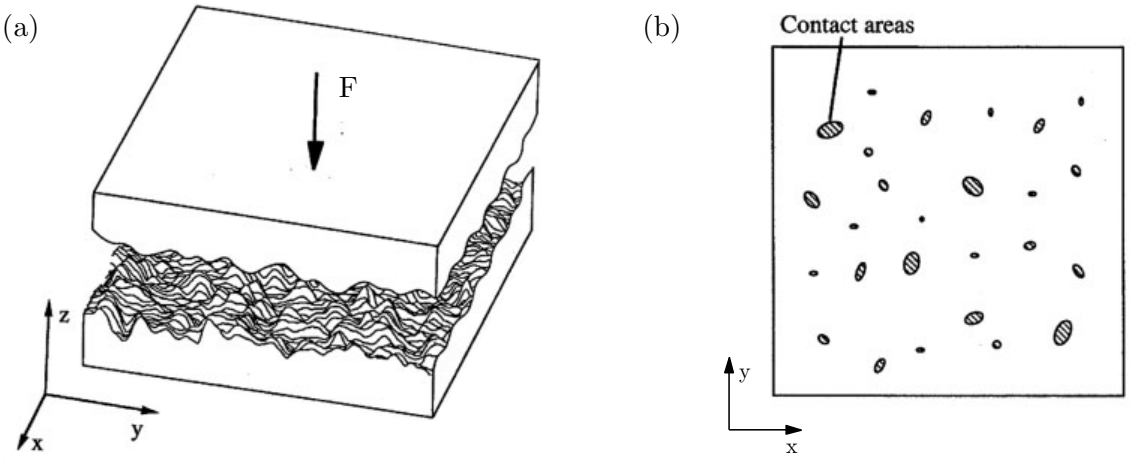

Figure 1.1: Illustration of (a) two rough surfaces being loaded against one another and (b) the points where the two surfaces come into contact, adapted from [10].

The process of measuring the topographical profile of a surface is called profilometry. Once a measurement has been made of the surface texture, the effect of waviness must be accounted for by applying a filter with a cutoff wavelength (L) to the measured profilometry data. A representative illustration of the resulting filtered data is shown in Figure 1.2. Waviness can be thought of irregularities that are larger than a cut off length. The cutoff length is the length of scale (measured parallel to the profile) necessary for irregularities to be observed. Waviness can be the result of tooling marks, residual stresses, or vibrations in measurement.

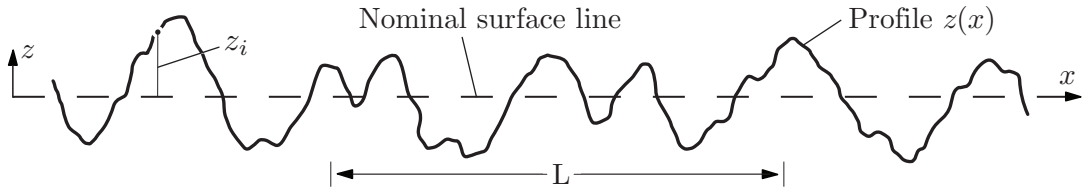

Figure 1.2: Illustration showing the roughness of a surface after filtering to remove the effect of waviness from a hypothetical surface profile.

Measurements of surface profiles are not continuous functions, they are discrete points of measurement (z_i) collected from an instrument. Roughness is quantified by a variety of parameters, including average roughness (R_a), root mean squared roughness (R_q), skewness (R_sk), and kurtosis (R_ku). R_a and R_q are measures of the average deviation and the root mean square average deviation of the measured profile from a nominal surface line respectively. R_sk is a measure of concentration of the deviations either above or below the nominal surface line and R_ku is a measure of how "sharp" those deviations are. The method of calculations these parameters is given by

$$\begin{aligned} R_\mathrm{a} &= \frac{1}{n}\sum_{i=1}^{n}|z_i| & R_\mathrm{q} &= \sqrt{\frac{1}{n}\sum_{i=1}^{n} z_i^2} \quad = 2 \\ R_\mathrm{sk} &= \frac{1}{nR_q^3}\sum_{i=1}^{n} z_i^3 & R_\mathrm{ku} &= \frac{1}{nR_q^4}\sum_{i=1}^{n} z_i^4 \end{aligned} \tag{1.1}$$

Precision components are often finished with very low surface roughness. For example, bearing races are typically polished to a level of $\mathrm{R_a}$ 0.025–0.05 µm or lower. For mechanisms, a very high surface finish is desirable, but a surface can be too smooth. Around $\mathrm{R_a} = 0.001$ µm surfaces in contact can suddenly seize.

1.2.1 Hertzian Contact Model

A simple analysis of a ball loaded on a plate would show that, theoretically the contact area between a sphere and a plane would be zero and the resulting pressure would be infinite for any nonzero force using the classic calculation of $p = F/A$. In reality, the ball and plate are both elastic bodies and will elastically deform at the their interface when they touch, creating a small contact area with a finite pressure. The Hertzian model of contact describes this elastic behavior and allows us to estimate the contact pressure. The localized contact stresses between curved surfaces are referred to as Hertzian contract stresses. The Hertzian contact model was first developed by Heinrich Hertz in 1882 to understand how the forces which hold multiple lenses together affect their optical properties. Today, the Hertzian contact model forms the foundation for the analysis of the load-bearing capacity of bearings, gears, and many other mechanisms.

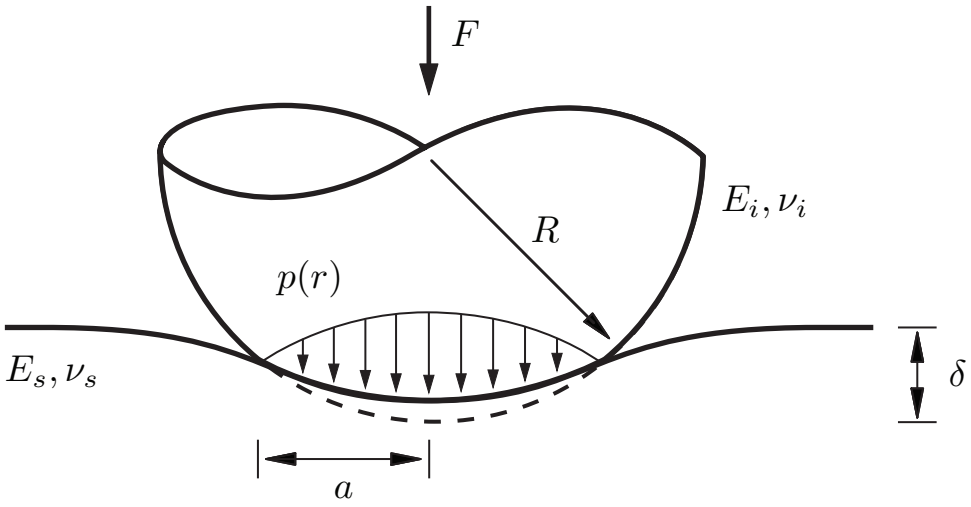

Figure 1.3: Ball-on-flat contact under load where the dashed lines show the undeformed profile of the ball.

The Hertz model neglects any the effect of adhesive and frictional forces on the bodies in contact. The ball-on-flat contact is modeled as an elastic spherical indenter loaded on a semi-finite elastic medium, as shown in Figure 1.3. The radius of contact (also called the Hertzian radius) a and the deflection δ are defined as

$$a = \left(\frac{3FR}{4E'}\right)^{1/3} \tag{1.2}$$

$$\delta = \frac{a^2}{R} = \left(\frac{9F^2}{16RE'^2}\right)^{1/3} \tag{1.3}$$

Where E' is the reduced modulus and is given by

$$E' = \left(\frac{1-\nu_s^2}{E_s} + \frac{1-\nu_i^2}{E_i}\right)^{-1} \tag{1.4}$$

The pressure distribution over the contact radius is given by

$$p(r) = p_0\left(1 - \frac{r^2}{a^2}\right)^{1/2}, \quad 0 \le r \le a \tag{1.5}$$

Where r is the radial distance from the center of the contact area and p_0 is the maximum contact pressure located at the center of the contact and is 150% the mean contact stress $\bar{p}$

$$p_0 = \frac{3}{2}\bar{p} = \frac{3}{2}\left(\frac{F}{\pi a^2}\right) = \left(\frac{6FE'^2}{\pi^3 R^2}\right)^{1/3} \tag{1.6}$$

1.2.2 Hertzian with a Thin Film

Since solid film coatings are readily used to lower friction and wear, there is a need to understand the contract pressure of ball-on-flat systems when a thin film is present. Hsueh and Miranda proposed a combined empirical and analytical method for predicting the behavior of a ball loaded on coating/substrate system, which can be modeled using a modified Hertzian contact model [11, 12].

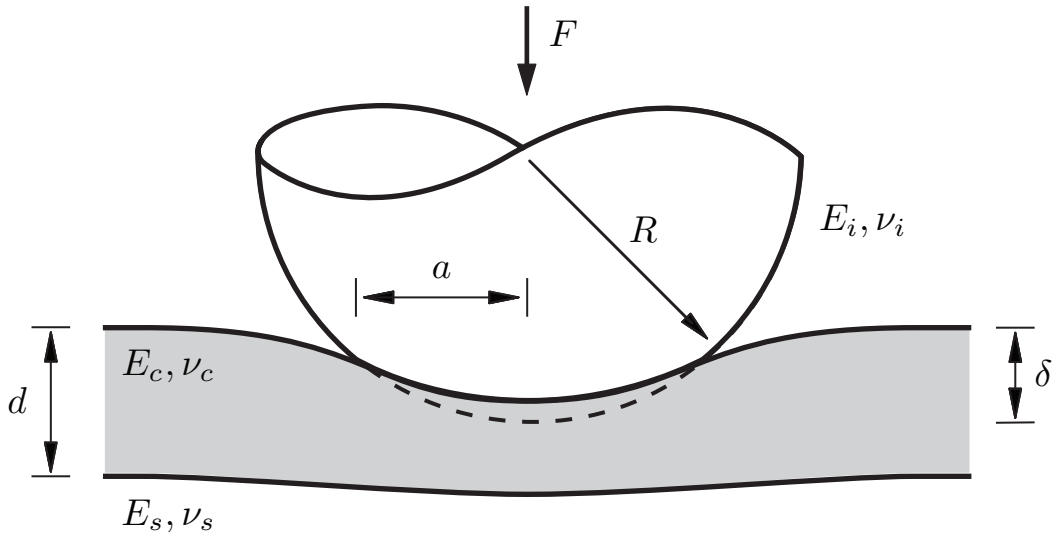

Figure 1.4: Ball indenter on a coating/substrate system.

First, consider an elastic ball indenting an infinitely thick coating where the contact area a_c and deflection δ_c are given by

$$a_c = \left(\frac{3RP}{4E'}\right)^{1/3} \tag{1.7}$$

$$\delta_c = \left(\frac{9F^2}{16E'^2R}\right)^{1/3} \tag{1.8}$$

Where E' is the reduced modulus of the ball coating system given by Equation (1.4). Both a_c and δ_c follow the standard Hertz model and be can be expressed in terms of each other by Equation (1.3)

$$a_c = \sqrt{R\delta_c}, \quad \delta_c = \frac{a_c^2}{R} \tag{1.9}$$

Next, treat the coating/substrate system as a homogeneous material with an effective elastic modulus ($E_{c/s}$) that is defined in terms of the elastic modulus of the

coating (E_c) modified by a parameter (ψ), i.e. $E_{c/s} = \psi E_c$. The derivation of ψ can be found in [12]. Then, the total contact area a_t, and total deflection δ_t, are given by

$$a_t = \left(\frac{3RP}{4E^*}\right)^{1/3} \tag{1.10}$$

$$\delta_t = \left(\frac{9F^2}{16{E^*}^2 R}\right)^{1/3} \tag{1.11}$$

Where E^* is the reduced modulus of the indenter and the combined coating/substrate system given by

$$E^* = \left(\frac{1-\nu_c^2}{\psi E_c} + \frac{1-\nu_i^2}{E_i}\right)^{-1} \tag{1.12}$$

Where ψ is given by

$$\psi = \left(1 + \frac{E_c(1+\nu_s)}{\pi E_s(1-\nu_c^2)}\left[(3-2\nu_s)\Lambda_1 + \Lambda_2\right] - \frac{1}{\pi(1-\nu_c^2)}\left[(3-2\nu_c)\Lambda_1 + \Lambda_2\right]\right)^{-1} \tag{1.13}$$

where Λ_1 and Λ_1 are functions of d/a_t given by

$$\Lambda_1 = \frac{\pi}{2}\left(1 + \frac{d^2}{a_t^2}\right) - \frac{d}{a_t} - \left(1 + \frac{d^2}{a_t^2}\right)\sin^{-1}\left[\frac{d}{a_t}\left(1 + \frac{d^2}{a_t^2}\right)^{-1/2}\right] \tag{1.14}$$

$$\Lambda_2 = -\frac{\pi}{2}\left(1 + \frac{3d^2}{a_t^2}\right) + \frac{3d}{a_t} + \left(1 + \frac{3d^2}{a_t^2}\right)\sin^{-1}\left[\frac{d}{a_t}\left(1 + \frac{d^2}{a_t^2}\right)^{-1/2}\right] \tag{1.15}$$

Unlike the previous example of indention on an infinitely thick coating, the assumption that $a = \sqrt{R\delta}$ is invalid for indention on coating/substate systems. Since the deflection and contact area cannot be expressed in terms of each other, they must be solved for independently. To solve this problem, Hsueh and Miranda developed an analytical model (which is the basis for the derivation of crefeqn:psi,eqn:Lambda1,eqn:Lambda2), that allows the use of the ratio of the deflection of the coating to the actual deflection as given by

$$\frac{\delta_t}{\delta_c} = \left(\frac{E^*}{E'}\right)^{2/3} \tag{1.16}$$

and using an empirical model an expression for the ratio of the coating to actual contact area is given by

$$\frac{a_t}{a_c} = \frac{1 - (E_c/E_s)^{1/3} - \dfrac{C_1(d/a_t)^{C_2}}{1 + C_3(E_c/E_s)}\left[1 - (E_c/E_s)^{C_4}\right]}{1 + C_5(d/a_t) + C_6(d/a_t)^3} \tag{1.17}$$

where C_1–C_6 are fitting parameters given by

$$C_1 = 0.666 \quad C_2 = 0.0261 \quad C_3 = 113.413$$
$$C_4 = 2.069 \quad C_5 = 2.8540 \quad C_6 = 3.143$$

can be used in conjunction with Equations (1.7) and (1.8) to find the pressure developed by a given load using the following procedure:

(i) Guess a_t

(ii) Calculate a_t/a_c and δ/δ_c from Equations (1.16) and (1.17)

(iii) Calculate a_c from Equation (1.7)

(iv) Calculate δ_c from a_c using Equation (1.9)

(v) Calculate δ_t from δ_c using Equation (1.16)

(vi) Calculate F from either δ_c or a_c using either

(vii) Iterate a_t and repeat steps (i) to (vi) until the resulting F corresponds to the desired mean pressure ($\bar{p} = F/a^2$) or maximum pressure ($p_0 = 1.5F/a^2$).

It should be noted that this procedure will overestimate contact pressure for the case of $E_c > E_s$, as the analytical model which is the basis for the derivation of Equation (1.16) neglects the effect of flexural stresses at the surface.

1.3 Lubrication Regimes

There are four regimes of lubrication that are recognized and distinguished by the behavior of the lubricant film thickness in each regime [13]. The regime can be determined by the dimensionless film parameter (λ) which is defined as the ratio of the the minimum film thickness (h_0) to the composite surface roughness (R'_q)

$$\lambda = \frac{h_0}{R'_q} \tag{1.18}$$

Where the lubrication regime can be identified as

$$\begin{aligned} \text{Boundary Lubrication,} \quad & \lambda < 1 \\ \text{Mixed Lubrication,} \quad & 1 < \lambda < 3 \\ \text{Elastohydrodynamic Lubrication,} \quad & 3 < \lambda < 5 \\ \text{Hydrodynamic Lubrication,} \quad & 5 < \lambda \end{aligned} \tag{1.19}$$

The composite surface roughness R'_q is defined for the purpose of calculating λ as the square root of the sum of squares of the R_q roughness parameter for both surfaces sampled with a cutoff wavelength of $2a$. Where a is contact radius from Equation (1.2) for ball-on-flat contacts.

$$R'_q = \sqrt{R_{q,A}^2 + R_{q,B}^2} \tag{1.20}$$

where:

$R_{q,A}$	is the R_q of body A with a filter cutoff wavelength of $2a$
$R_{q,B}$	is the R_q of body B with a filter cutoff wavelength of $2a$

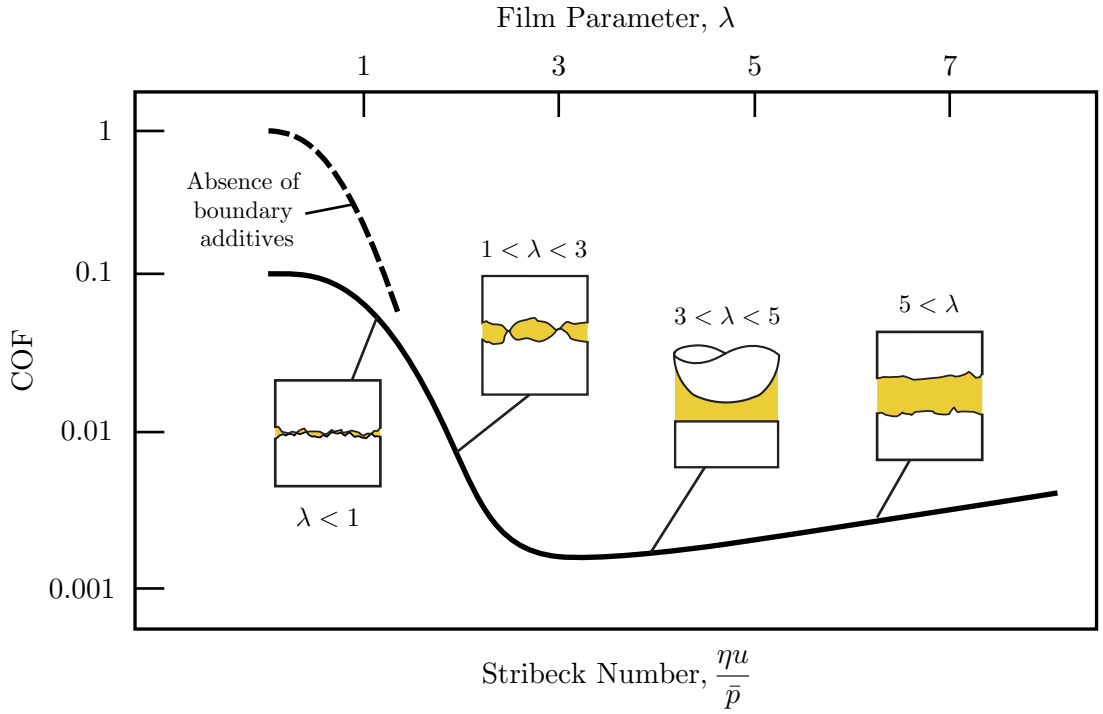

Figure 1.5: Illustrative plot showing the coefficient of friction as a function of the Film Parameter (λ) and the Stribeck Number, adapted from [13, 14]

The minimum film thickness can be estimated up to contact pressure of 3 GPa using the numerically derived formulae from Hamrock and Dowson [15].

$$h_0 = 3.63R\left(\frac{u\eta_0}{E'R}\right)^{0.68}\left(\alpha E\right)^{0.49}\left(\frac{F}{E'R^2}\right)^{-0.073}\left(1 - e^{-0.68k}\right) \tag{1.21}$$

where:

h_0 is the minimum film thickness [m]
u is the the entraining surface speed [m/s]
η_0 is the the lubricant viscosity at atmospheric pressure [Pas]
E' is the reduced young's modulus from Equation (1.4) [Pa]
R is the is the radius of the ball [m]
α is the is the pressure-viscosity coefficient [m^2/N]
F is the contact load [N]
k is the ellipticity parameter ($k = 1$ for circular contact)

1.4 Traditional Bearing Materials

Materials which are used to manufacture bearings, gears, and other mechanical components have an ideal set of properties that ensure high tribological performance. These materials should be very hard and have high strength and thermal conductivity. To be used in precision mechanisms, a material must be able to be manufactured to tight tolerances with controlled surface finishes, and maintain dimensional stability while resisting corrosion. In applications involving sensitive instrumentation, it is important that materials are nonmagnetic and are electrically conductive for the dissipation of static charge [16]. No traditional bearing material encompasses all of these desirable properties, which has motivated a search for new bearing materials.

High carbon and chromium steels like 52100 are widely leveraged for their high hardness and resistance to rolling contact fatigue. However, these steels are highly susceptible to corrosion and their applications are limited to controlled environments. Martensitic stainless steels like 440C have comparably high hardness and wear resistance while enjoying higher corrosion resistance. But despite being labeled stainless, 440C still suffers from corrosion and could more accurately be referred to as a "corrosion resistant" steel rather than a true stainless steel. Additionally, ferrous materials are highly magnetic and have relatively high densities which create large centrifugal forces at high speeds when used for rolling elements, thus limiting fatigue life.

Ceramics like silicone nitride (Si_3N_4) are very hard and have good wear resistance, but are not susceptible to corrosion like steels are. Additionally, they are nonmagnetic and have low densities, making them ideal materials for rolling elements in high speed applications. However, ceramics are not electrically conductive (insulators) and have mismatched coefficients of thermal expansion with traditional structural materials. This mismatch in thermal properties, combined with the brittleness of ceramics, precludes their use in many applications due to the weakness of ceramics to cyclic fatigue stress, that is caused by the mismatched expansion and contraction of mated parts during temperature changes.

1.5 Near-equiatomic Nickel Titanium or "NiTiNOL" Alloys

The NiTiNOL family of alloys are a range of near-equiatomic Nickel-Titanium (NiTi) alloys best known for their super-elastic properties and for exhibiting the Shape Memory Effect (SME). The name "NiTiNOL" comes from the Naval Ordnance Laboratory Research (NOL), where William J. Buehler and his colleagues both discovered and led the pioneering research on NiTiNOL alloys in the late 1950's [17–20]. The word NiTiNOL is itself an acronym for "Nickel Titanium Naval Ordnance Laboratory." While the name NiTiNOL most commonly refers to alloys that exhibit the SME, when Buehler discovered NiTiNOL, he identified two different compositions of interest—approximately 55 wt% Ni and a more Ni-Rich 60 wt% Ni, designated 55NiTi and 60NiTi respectively. Buehler described 60NiTi as a "non-magnetic precipitation hardenable tool-like material" and was fascinated by the SME properties of 55Niti. While 55NiTi was soft and easy to work, 60NiTi was found to be prone to excessive work hardening and was determined to be prohibitively difficult to manufacture. The NOL abandoned early research on 60NiTi in the early 1960's due to lack of resources and in favor of the more interesting SME properties of 55NiTi [20].

In August of 2004, Dr. Chris Dellacorte from NASA Glenn Research Center was approached by Glenn Glennon of Abbott Ball Co. with the idea to use Ni-rich NiTi alloys for bearing materials. Unlike lower nickel content 55NiTi, it has been shown that with an appropriate heat treatment, 60NiTi could be tailored create an extremely hard, weak-ordered intermetallic alloy that does not exhibit shape memory behavior. Since then, there has been a considerable research effort at NASA Glenn to develop the 60NiTi alloy for structural and mechanical applications, most notably rolling element bearings [16, 20–51].

Traditionally, bearing materials are both very hard and very stiff. These two properties have typically been considered to be linked. However, 60NiTi is both relatively hard (56–62 HRC) after appropriate heat treatment, but relatively less stiff ($E = \sim 100$ GPa) compared to traditional bearing materials. In the 1950s, Oberle suggested that the ratio of a material's hardness to its stiffness, designated the Modell factor, could predict machine life of components made from that material [25, 52]. While high hardness is advantageous for wear resistance, high stiffness means higher local contact pressures and higher likelihood of Brinell damage in the event of an overloading event. The rough uneven features created by Brinell denting in a bearing raceway can cause premature fatigue failure of the bearing. Therefore, a material with a high ratio of indentation hardness to elastic modulus would have high wear resistance as well as low local contact pressures, which would reduce the likelihood of Brinell damage. When Oberle first made this prediction, no high Modell number materials were available, but now 60NiTi is one such material [25].

In addition to having a high Modell factor, 60NiTi has exhibited incredible dent resistance and resilience, with reported recoverable strains over 5%, significantly greater than steels, which will show permanent deformation at just 1% strain [33]. Furthermore, 60NiTi has shown an extremely high coefficient of restitution [53]. 60NiTi can be machined to high tolerances and surface finishes prior to heat treatment, and unlike NiTi55, 60NiTi does not show a martensitic transformation until over ~ 100 ℃, which gives it sufficient dimensional stability to be used to manufacture components of precision mechanisms [54]. 60NiTi is conductive but nonmagnetic, and unlike ceramics, has a coefficient of thermal expansion similar to other structure materials so that is not grossly mismatched with that of components it may be mated with. Additionally, NiTi has a modest density of 6.7 g/cm^3 which is $\sim 15\%$ lighter than steel, and 60NiTi is so inherently resistant to corrosion that Dellacorte referred to it as corrosion "proof" [16, 35]. This set of properties unique to 60NiTi make it a highly promising candidate for a bearing material. The differences in selected material properties of 60NiTi and representative martensitic stainless steel (400C), high carbon chromium steels (52100), and ceramics (Si3N4) are summarized in Table 1.1.

Table 1.1: Tabulated comparison of selected technical properties of 60NiTi and several traditional bearing materials, adapted from [36].

Property	60NiTi	440C	52100	Si_3N_4
Density (g/cm^3)	6.7	7.7	7.81	3.2
Hardness	56–62 HRC	58–62 HRC	60–63 HRC	1300–1500 Hv*
k (W/m·K)	$\sim$ 9–14	24	46.6	33
α ($\times 10^{-6}$/℃)	~ 10	10	12.5	2.6
ρ ($\times 10^{-6}\,\Omega$·m)	~ 1.04	~ 0.60	0.22	Insulator
Magnetic	No	Yes	Yes	No
Corrosion resistance	Excellent	Marginal	Poor	Excellent
E (GPa)	~ 100	200	210	310
Poisson's ratio, ν	~ 0.34	0.3	0.3	0.27
Modell factor†	0.62	0.31	0.3	~ 0.24

*Vicker's hardness (Hv) is a hardness scale for ceramic materials with values beyond HRC 75

†Calculated as the ratio of the hardness in HRC to the elastic modulus in GPa

1.6 Research and Development of 60NiTi

While 60NiTi was once considered prohibitively difficult to manufacture, there have been many advances in powdered metallurgy techniques since Buehler first discovered in the late 1960s that allow useful quantiles of quality 60NiTi to be readily produced. Research is still ongoing into different techniques for primary processing as development of the alloy continues. Casting of 60NiTi often results in voids, inclusions, tramp carbon impurities, and unconsolidated particles of Ni or Ti. Additionally, quenching 60NiTi during heat treatment imparts large amounts of internal stress. The intrinsic brittleness, combined with defects in casting, greatly degrades the performance of 60NiTi and increases its susceptibility to cracking during heat treatment. An alternative method, which has been shown to produce much higher quality material than casting, is the consolidation of gas atomized Ni and Ti particles by hot isostatic pressing (HIP) [39]. HIP reduces defect sizes to that of the powder particle size and produces a more homogeneous and high quality material with isotropic properties. This is due to the random orientation of the particles during HIP processing [39].

In the process of developing 60NiTi, it was discovered that the addition of 1 atomic percent hafnium to 60NiTi increases the uniformity of and reduce flaws in the microstructure of the alloy, (Figure 1.6), by acting as a "getter" for contaminants [36]. The exact composition by weight percent is 57.6 wt.% Ni, 39.2 wt.% Ti, and 3.2 wt.% Hf, and the resulting alloy is designated NiTi-Hf. The addition of Hf also made 60NiTi dramatically less susceptible to cooling rates during heat treatment and subsequently less likely to crack during quenching. The addition Hf has also been shown to increase rolling contact fatigue resistance and enable 60NiTi to endure higher stress levels, likely due to the improved homogeneity in microstructure and reduction of voids, inclusions, and other flaws during processing [36, 55]. The inclusion of Hf leads to such dramatic improvements in processability and load bearing capabilities that future iterations of fully developed 60NiTi bearing components will likely be of a NiTi-Hf composition [36].

Titanium and titanium rich alloys are notorious for poor tribological performance even when well lubricated [20, 56]. Ti-6Al-4V for example, exhibits galling even under oil and grease lubrication. 60NiTi and NiTi-Hf have both been shown to exhibit relatively inferior sliding wear resistance as compared to 440C, under unlubricated conditions [57, 58]. The performance of titanium alloys in sliding is so poor that it was previously thought that the only effective means of preventing adhesive wear (galling) in titanium sliding contacts was the use of fluorocarbon dry films such as polytetrafluoroethylene (PTFE) [59]. Gears made from 60NiTi that were coated with both a PTFE and with a graphite filled PTFE solid lubricant coating were evaluated, and it was shown that they had low friction but high wear [37]. However, [60] showed that with proper surface preparation, PTFE solid film coatings bonded to 60NiTi substrates by polydopamine (PDA) adhesives can have long life

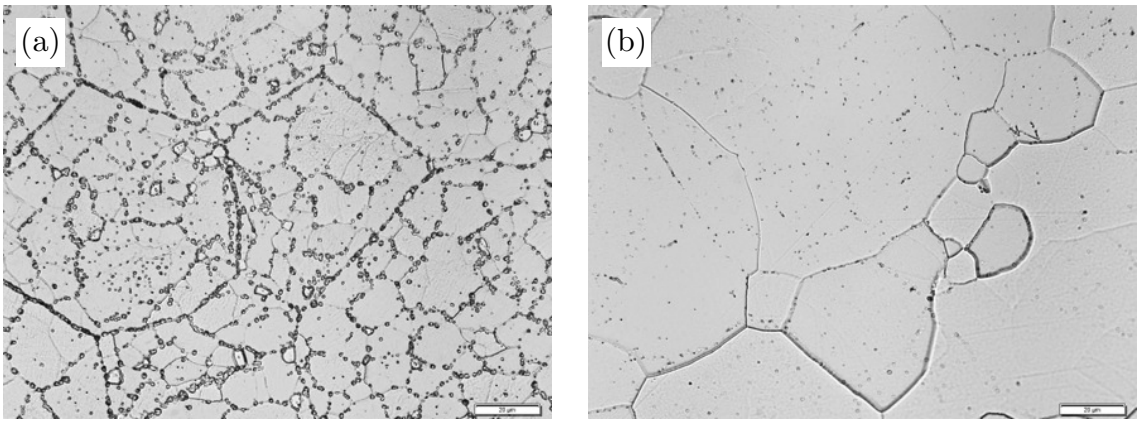

Figure 1.6: optical microscope pictures of the microsctructure of (a) 60NiTi produced by HIP and (b) NiTi-Hf produced by HIP showing the reduction of flaws [44].

sliding against Si_3N_4 and show potential as a solid lubricant for 60NiTi. The use of surface nitriding and anodization, in conjunction with dry film lubricant coatings has been proposed as a way to reduce friction and protect titanium rich substrates from wear [61]. Studies have shown that plasma nitriding of NiTi-Hf improved wear resistance in dry sliding as compare to untreated NiTi-Hf [49, 51]. Additionally, the effects of laser shock penning and ultrasonic crystal surface modification of NiTi alloys was shown to increase scratch hardness of NiTi alloys [62, 63].

Titanium rich alloys, including Ti-6Al-4V, are known not only to be unsuccessfully lubricated by oils, but to be chemically aggressive toward oils and cause them to degrade [20, 56]. Given that Ti rich alloys perform so poorly under lubrication, and that components made from 60NiTi/NiTi-Hf will likely operate with a lubricant, it is vital to study how to properly lubricate 60NiTi/NiTi-Hf. It has been shown that in rolling sliding contact perfluoropolyether (PFPE) and multiply-alkylated cyclopentane (MAC) oils can successfully lubricate 60NiTi [16, 20–22, 25]. Friction and wear tests have been performed using castor oil, turbine oil, and paraffin oil where castor oil was found to exhibit ultra low friction and lower wear compared to the other oils [64–67]. 60NiTi and NiTi-Hf were evaluated using fully formulated synthetic (PAO) gear oil, and showed that under the same conditions 440C, was better lubricated [57, 58]. Further, investigations examined the intentional work hardening of a 60NiTi sample that was not hardened by heat treatment during sliding lubricated with cubic boron nitride (CNB) and MoS_2 additized mineral oil grease [68]. This study showed that both additives could be effective at reducing wear and that the intentional work hardening of the surface has potential for future development. Yet, there has still not been a thorough investigation into the factors that control the reported performance of castor oil for lubricating 60NiTi or a thorough evaluation of the ability of different greases to lubricate 60NiTi.

1.7 Summary, Motivation, and Research Objectives

Titanium rich alloys are known to have poor tribological performance and to be chemically aggressive toward lubricants. Since 60NiTi is a titanium rich alloy, and components made from 60NiTi will likely operate with a lubricant, it is vital to study how to properly lubricate 60NiTi contacts. This thesis is concerned with the evaluation of the performance and ability of several lubricants to lubricate NiTi-Hf components. The work presented here is the result of a series of tests and investigations conducted on samples of NiTi-Hf donated by NASA Glenn Research Laboratory (shown Figure 1.7). The goal of this research is to characterize the performance of NiTi-Hf sliding contacts with different lubricants at a range of operating conditions. This first chapter serves to provide and clarify the relevant background concepts and information integral to the work presented later in this document. Chapter 2 contains explanations of all test equipment and methods used for collecting and processing test data. Chapter 3 contains the results and discussion of a study on the effect of pressure and roughness on friction in caster oil lubricated NiTi-Hf/steel contacts. Chapter 4 contains the results and discussion of a study that evaluated the performance of five different greases in terms of their ability to lubricating NiTi-Hf. Chapter 5 contains a discussion on recommendations for future studies.

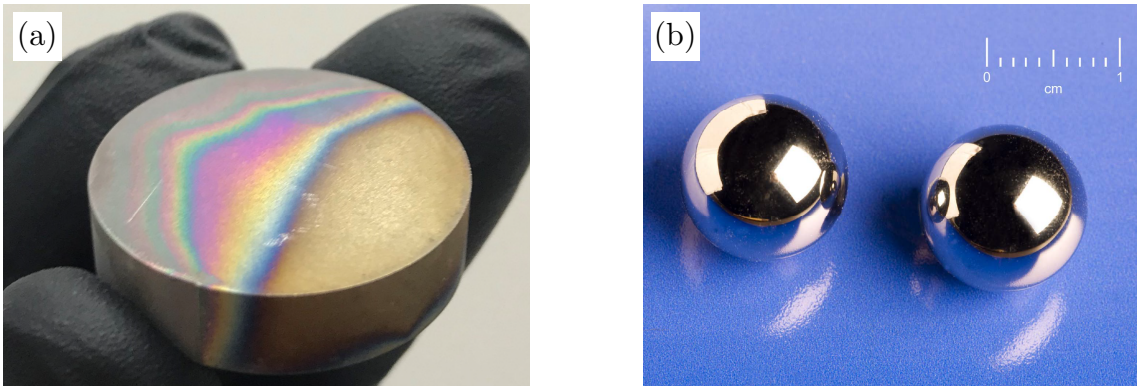

Figure 1.7: Pictures of (a) as received NiTi-Hf sample used in this study that were processed by HIP and provided by NASA Glenn Research laboratory, (b) polished 60NiTi balls from [20].

Chapter 2

EXPERIMENTAL DESIGN

2.1 Tribological Testing

To empirically study friction and wear, quantitative measurements are required. These measurements can be collected in a controlled laboratory environment by a device called a tribometer. Typical laboratory tribometer configurations consist of a ball or a pin with a spherical cap loaded onto a disk or flat sample which slides or rotates to create relative motion. These test configurations, shown in Figure 2.1 are referred to as ball-on-flat or ball-on-disk testing.

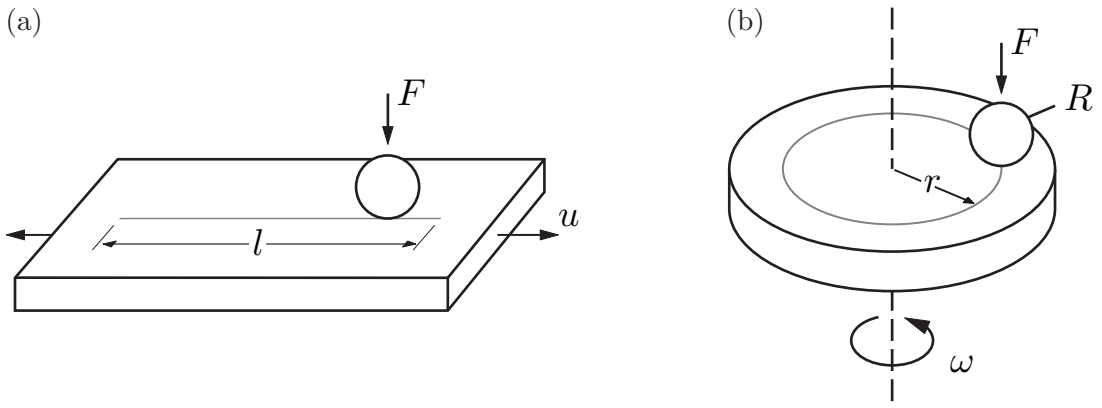

Figure 2.1: Illustration of (a) linear reciprocating ball-on-flat testing and (b) unidirectional ball-on-disk test configurations.

When testing is performed to inform a real world application, it is best to study the performance of the system in the actual geometry and environment that it will experience in use. However, field tests are usually extremely complicated, time-consuming, and can be prohibitively expensive. For this reason, the use of laboratory testing is widely employed. When designing a tribological laboratory test, significant care is required to ensure the test conditions recreate the real world application. For example, in the case of studying wear, laboratory tests can generally only be extrapolated to real world conditions when the wear mechanisms are expected to be similar [69]. Therefore, pin-on-disk testing is often only used to evaluate the relative performance of a different materials under similar test conditions.

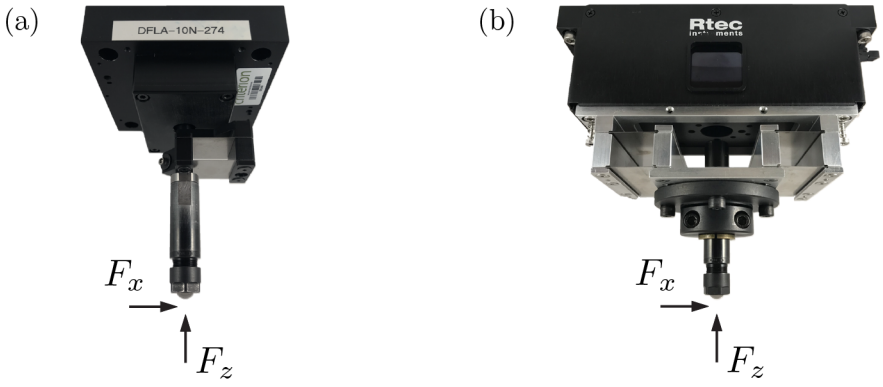

Figure 2.2: Rtec Instruments load cells setup with a 3/8" inch ball loaded in collect chucks which are held in the (a) Low Newton Load Cell and (b) Medium Newton Load Cell.

The normal force is sometimes applied by means of a deadweight, but can be actively controlled as well. Load cells are typically used to capture the frictional force. Two instruments from a Rtec Instruments tribometer are shown in Figure 2.2, that can regulate a constant normal force using a cantilever loading mechanism as well as capture the normal and friction forces that the ball or pin experience during sliding using two different load cells.

2.2 Capturing the Stribeck Curve

Stribeck curves were captured by running tests that start at high sliding speeds to ensure full-film lubrication. The speed was then decreased in steps for constant pressure and the COF was averaged for each step, as shown in Figure 2.3.

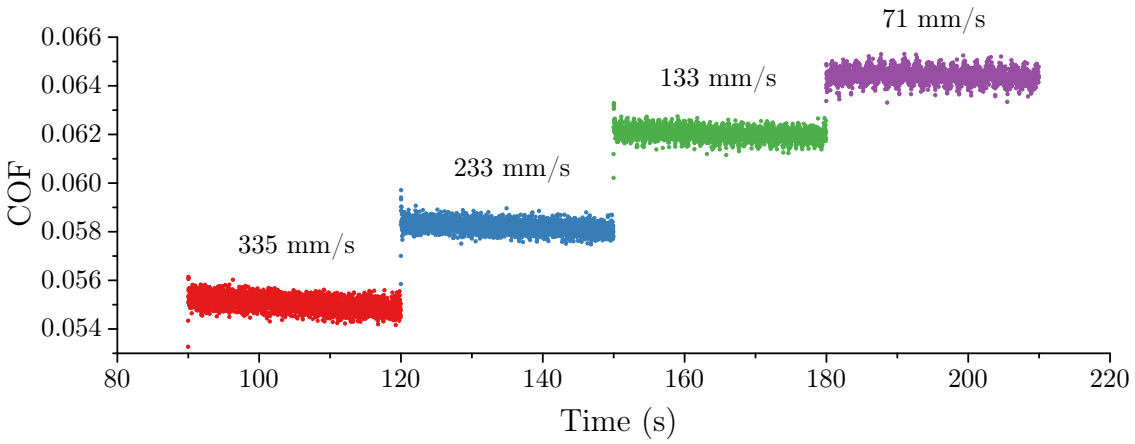

Figure 2.3: Representative friction vs. time data illustrating the test process in which the speed was decreased in a stepwise fashion to generate a stribeck curve.

2.3 Calculation and Measurement of Wear on the Flat

The wear scars were measured using a white light interferometer, which captureed high resolution 3D images of wear scars as shown in Figure 2.4.

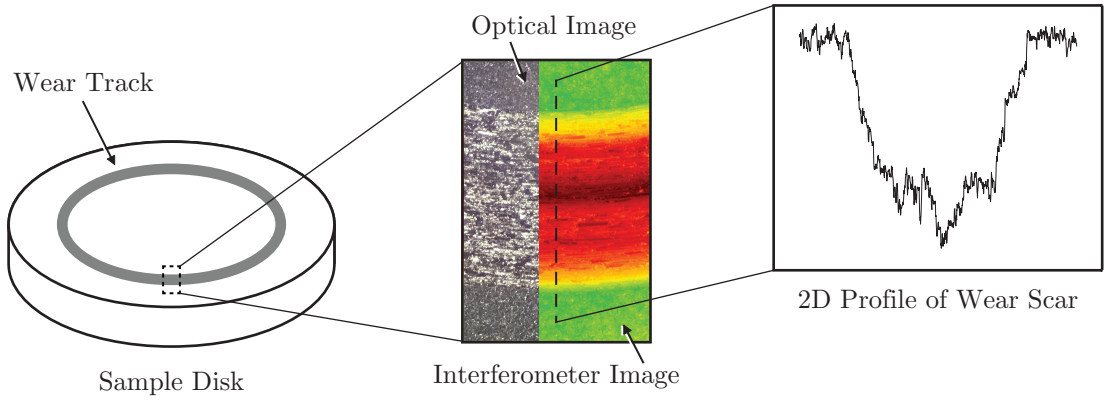

Figure 2.4: Interferometer wear track imaging

The wear volume was calculated as the average of the cross-sectional wear area of six profiles along the wear scar multiplied by the length of the scar. The cross-sectional wear was defined as the difference between the areas above and below the average height of the surface [70], as shown in Figure 2.5. It should be noted that if protruding features were present, the area above the average surface height was increased, and the calculated wear volume was decreased.

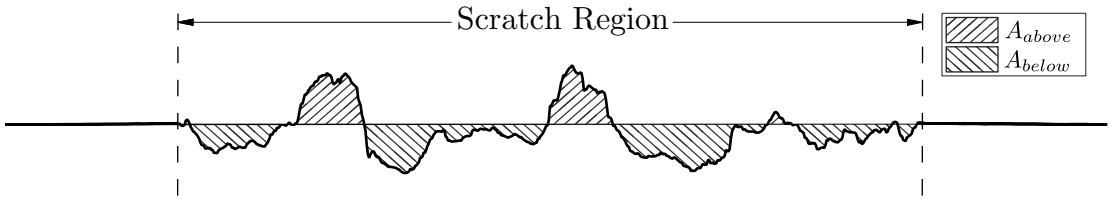

Figure 2.5: Schematic illustration of the wear calculation for a cross sectional profile of a flat that has protruding features above the surface line.

2.4 Calculation and Measurement of Wear on the Ball

For small wear cases, wear volume was calculated as the difference between the volume of an unworn ball and that of a worn ball measured by interferometry over the entire scar area, as illustrated in Figure 2.6. In cases where the wear on the ball was too severe to calculate with this approach, the wear volume was approximated using a spherical cap with a base radius that is the same as the radius of the wear scar as described in [51].

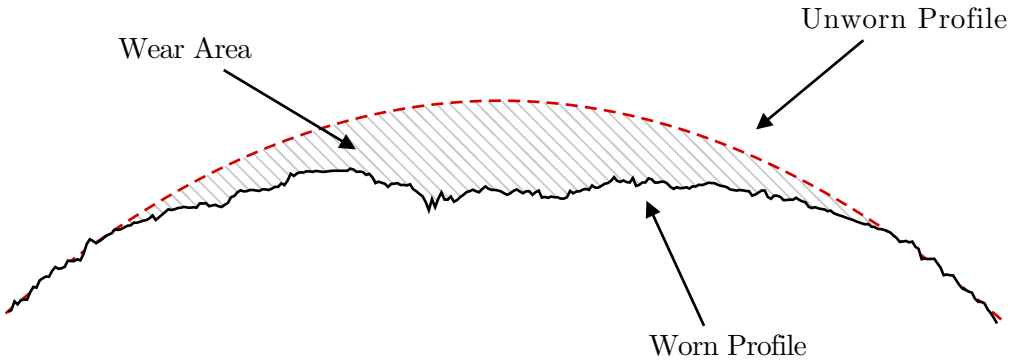

Figure 2.6: Schematic diagrams illustrating the wear calculations for the ball

2.5 Sample Preparation

All samples were prepared using an Allied High Tech Metprep 3 polisher. To achieve high surface finishes, the samples were first are run against a silicon carbide abrasive pad at 120 grit until no marks from machining were visible. Then the samples were polished with a progression of 320, 600, and 1200 grit silicon carbide abrasive paper, lubricated by water. Finally, the sample are polished against a firm back cloth platen saturated with a 6 µm polycrystalline diamond abrasive in a hexylene glycol suspension until the desired surface finish is achieved.

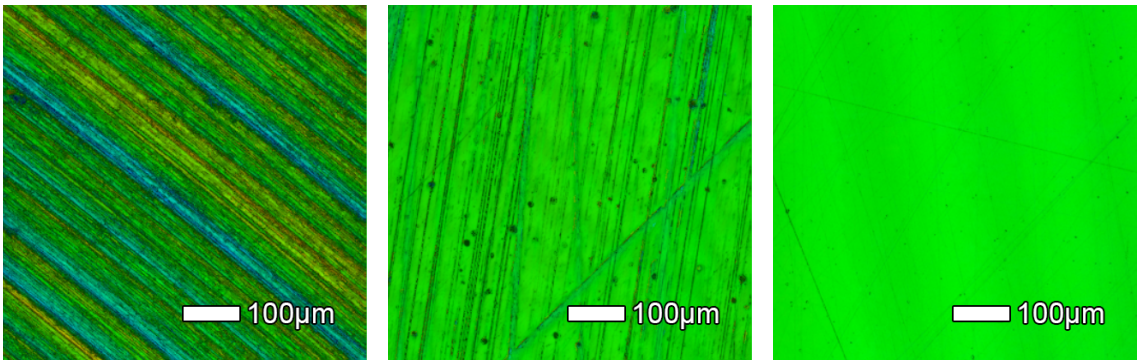

Figure 2.7: Interferometer images of a surface that has (a) been faced on lathe with carbide bit to $R_a = 266.8 \pm 48.30$ nm (~ 8 µin), then polished with (b) 120, 320, 600, 1200 grit silicon carbide abrasive paper lubricated with water to $R_a = 30 \pm 5.43$ nm (~ 1 µin), then finished with (c) 6 µm polycrystalline diamond abrasive suspended in hexylene glycol to a surface finish of $R_a = 1.62 \pm 0.07$ nm (~ 0.25 µin).

Chapter 3

THE EFFECT OF ROUGHNESS ON SUPERLUBRICITY FOR CASTOR OIL LUBRIACTED 60NITI

3.1 Castor Oil as a Lubricant for 60NiTi

There has been a series of recent studies conducted to characterize the performance of castor oil as a lubricant for 60NiTi [55,65–67]. The interest in castor oil is that it is a "green" lubricant. Castor oil has long been recognized as a lubricant and had a range of applications before mineral oils and synthetic esters were widely adopted as lubricants [71]. Castor oil has been shown to exhibit better friction and greater load carrying capacity in an unformulated form than commercial oil and to have oxidative stability and anti wear performance comparable to commercial oil when formulated with suitable additives [71, 72].

3.2 Superlubricity under Castor Oil Lubrication

Recent studies of castor oil lubricated 60NiTi-GCr15 contacts showed that superlubricity was achievable under specific conditions [66, 66]. Specifically, a COF of 0.004 was measured for a 60NiTi pin sliding against a GCr15 (Chinese equivalent of AISI 52100) disk with a hertzian contact pressure of 280 MPa. The results were explained by a proposed tribochemical reaction which resulted in the formation of a protective tribofilm [67]. It was proposed that the castor oil degrades to yield an interface with layers of hexanoic acid bonded to layers of nickel oxy-hydroxide and iron oxy-hydroxide. It was suggested that the repulsive electrostatic interactions between these intercalated layers enabled low resistance to shear and therefore lead to the observed superlubricity as shown in Figure 3.1.

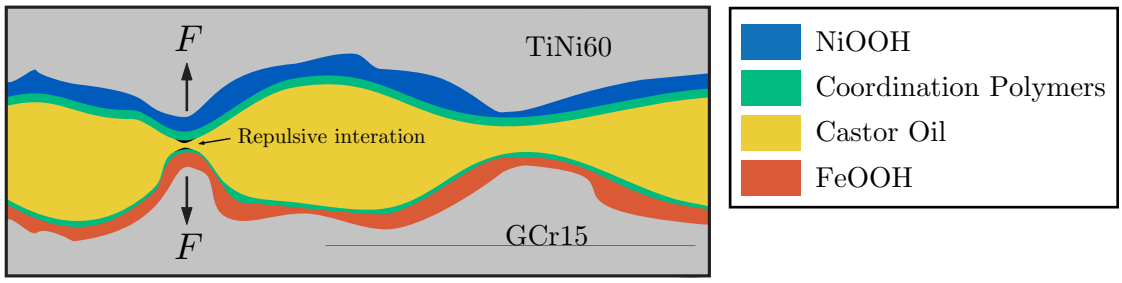

Figure 3.1: Illustration of the proposed protective tribofilm, adapted from [67]

3.3 Characterization of the Effect of Pressure and Roughness on Castor Oil Lubricated NiTi-Hf

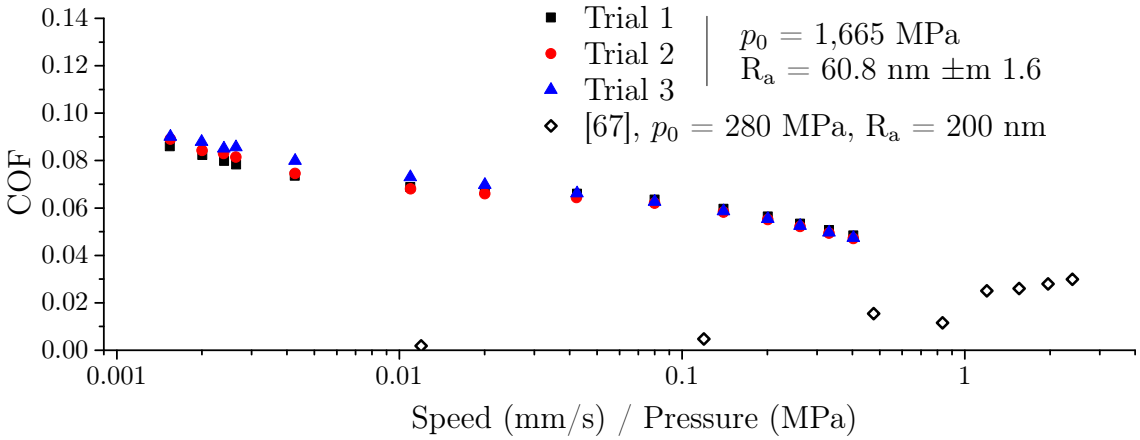

Figure 3.2: Average friction at each speed for three independent tests with as-obtained NiTi-Hf balls (solid symbols). Also shown are results obtained with a pin-on-flat geometry in [67] (hollow symbols).

Here, castor oil lubricated NiTi-Hf contacts sliding against AISI 52100 steel flats are characterized under a range of speeds, pressures, and surface finishes. Contact geometries include both ball-on-flat and a "flattened" ball which more closely approximates the large contact radius of the pin-on-disk set up used in [67]. The first set of measurements collected were performed with an as-received NiTi-Hf ball sliding on a polished 52100 steel disk. The average roughness (R_a) of the ball and disk were 60.8 ± 1.6 nm and 1.62 ± 0.2 nm, respectively, where the error corresponds to the standard error of the measured roughness data. A 30 N normal load corresponded to a maximum Hertz pressure of 1,665 MPa.

A representative data set from one trial is shown in Figure 3.2, where the speed was decreased stepwise and the friction was allowed to reach steady state at each speed as described in Section 2.2. The average friction coefficient at each speed is plotted as a function of the ratio of speed to pressure in Figure 3.2. This representation of the data is comparable to a Stribeck curve since all tests were performed at the same load and with the same castor oil lubricant, i.e. same viscosity. The results of the three independent tests were consistent and exhibited COFs decreasing from 0.09 to 0.05. These results are in contrast to those reported in [67] (also shown in Figure 3.2) where the COF increased with increasing speed and reached a value as low as 0.004. Two possible explanations for this difference are the geometry, i.e. ball vs. large contact radius pin, and contact pressure, i.e. 1,665 MPa vs. 280 MPa. It should be noted that the authors in [67] use a cast 60NiTi pin which may contain tramp carbon impurities, and here a NiTi-Hf ball produced by HIP is used.

3.3.1 Reducing Contact Pressure with the use of "Flattened" Spherical Caps

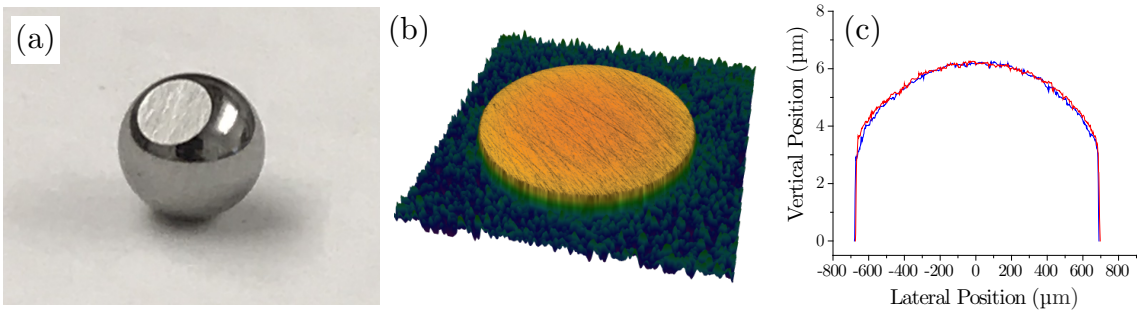

Figure 3.3: (a) Photo of a NiTi-Hf ball after being subjected to severe wear in order to obtain a much larger effective radius for subsequent friction testing. (b) White light interferometer image of the flat region on the ball. (c) Cross-sections of a representative flattened ball showing the large radius produced using the pre-test wear method where the red and blue lines correspond to measurements in two orthogonal directions.

From the Hertz contact theory, all else held constant, pressure is inversely proportional to the radius of the ball ($p_{max} \propto 1/R$). In order to lower the contact pressure and minimize the differences between the current experiments and those reported previously, the NiTi-Hf balls were subjected to severe wear in a controlled process to generate spherical caps of larger effective radius on the tip of the NiTi-Hf balls. The process entailed sliding the spherical balls on compliant silicon carbide abrasive paper. The wear was allowed to continue until the ball was flattened, as shown in Figure 3.3(a). White light interferometer profilometry analysis of the flattened region showed that the edges of the worn region were rounded, effectively corresponding to a much larger radius (see Figure 3.3(c)). This rounding is attributable to the fact that the abrasive paper was compliant, such that the paper wrapped around the edges of the contact during polishing. The effective radii of the flattened balls were determined using a least squares fit of a circle to the profile of the worn balls. The resulting radii of the flattened 2.38 mm radius NiTi-Hf balls with this method varied from 62 to 243 mm. The resultant geometry was similar to the 60NiTi pins used in [67] and enabled experiments to be performed at much lower Hertz pressures than what is shown in Figure 3.2. The roughness increased to 257.3 $\pm$ 27.3 nm, where the average and standard deviation were obtained from measurements of the three balls used to obtain the data in Figure 3.4.

Friction experiments were run with the flattened balls at a normal load of 30 N, corresponding to a Hertz pressure of 120 $\pm$ 14 MPa. The results are shown in Figure 3.4. Although the pressure range and geometry are now comparable to

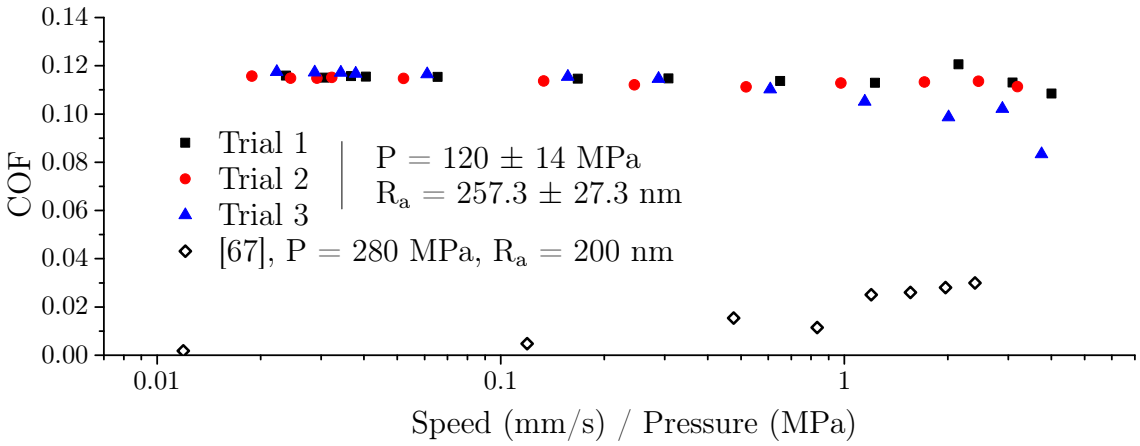

Figure 3.4: Friction results obtained with flattened NiTi-Hf balls having large effective radii which enabled much lower pressures to be achieved. Data reported from three independent tests (solid symbols). Also shown are results obtained with a pin-on-flat geometry in [67] (hollow symbols).

those reported in [67], the measured friction is still much higher. Also, the friction in the present experiments decreases with increasing speed while the friction in the previous study increases with increasing speed.

3.3.2 Lowering Surface Roughness with Varied Degrees of Polishing

In a lubricated contact, surface roughness can determine the lubrication regime based on its magnitude relative to the lubricant film thickness as described in Section 1.3. In order to further characterize the parameters that effect the friction in this contact, the same procedure for creating flattened balls described in Section 3.3.1 was preformed using different grits of silicon carbide abrasive paper to create a range of surface finishes. This created a total of twelve flattened balls with varying effective radii and roughness. At the constant load of 30 N, the effective radii corresponded to Hertz pressures between 87 and 258 MPa. The average roughness varied from 17.2 to 279.6 nm. Profiles of three representative flattened balls polished to different roughness scales are shown in Figure 3.5. Each surface was characterized by the average roughness, as well as the root-mean-square roughness (R_q), skewness (S_k), and kurtosis (K_u) which are described in further detail in Section 1.2. A summary of the ball radii and all roughness parameters is given in Table 3.1.

R_q was larger than R_a in all cases, but trended the same, so only R_a is reported subsequently. The skewness was slightly below zero for all cases, with an average value of $S_{k,ave}$ = -0.7, indicating surfaces with more valleys than peaks, typical of polishing [73]. The kurtosis was larger than three for all cases, with

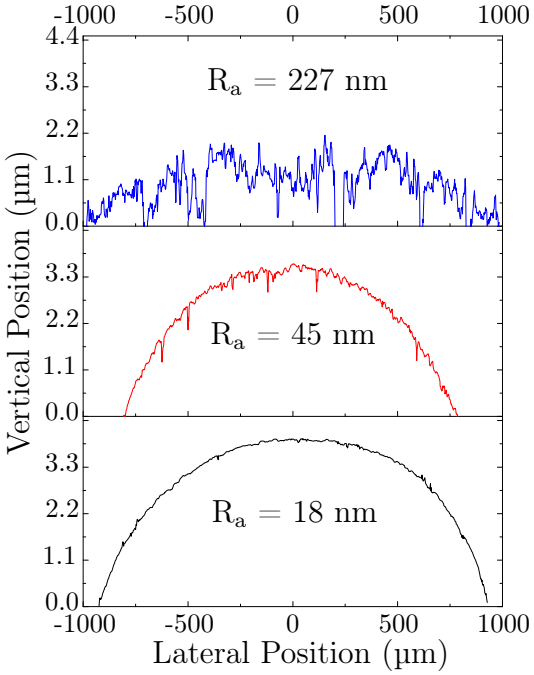

Figure 3.5: Cross-sections of representative flattened balls polished to different levels of roughness.

Table 3.1: Effective radius and roughness parameters for twelve flattened balls polished to varying degrees of roughness. Sorted by ball radius.

Ball	R (mm)	R_a	R_q	S_k	K_u
1	47.8	34.9	48.0	-1.0	7.3
2	62.3	17.7	25.3	-0.7	8.0
3	68.9	29.8	39.9	0.0	4.8
4	72.1	39.5	54.2	-0.5	6.4
5	89.9	30.1	40.1	-0.5	5.0
6	99.9	45.4	65.1	-1.5	9.5
7	115.6	17.2	26.5	-0.1	14.2
8	127.6	226.9	313.2	-0.9	7.0
9	138.6	36.4	51.1	-0.7	8.0
10	158.3	279.6	376.2	-0.7	6.2
11	175.2	265.5	366.4	-0.8	7.1
12	243.4	17.7	25.3	-1.0	8.3

an average value of $K_{u,ave} = 7.6$, indicating surfaces with sharp asperities. No correlation between these two parameters and the observed friction was found, so they will not be discussed further here.

Tests were run for each ball across the same range of speeds reported in Figures Figure 3.2 and Figure 3.4. However, to facilitate comparison between the various cases, study was focused on the friction at a speed of 31.1 ± 1.8 mm/s, which is near the speed of interest where super lubricity is reported in [67] at 33.4 mm/s. Average friction as a function of effective Hertz pressure for the original three balls (from Figure 3.2), the flattened balls, and from [67] is shown in Figure 3.6. The friction did not change monotonically with pressure. However, the roughness of the contacts varied significantly: the original ball roughness was 60.8 ± 1.6 nm, the flattened ball roughness ranged from 17.2 to 279.6 nm, and the roughness reported in [67] was 200 nm. Both pressure and roughness can affect the lubrication regime, which determines the friction mechanism, as discussed next.

3.3.3 The Effect of Pressure and Roughness on Lubrication

For the contact in the present study, the effective radius R varies for each flattened ball, the speed u is 31.1 mm/s, the reduced elastic modulus E' is 164.6 GPa, the pressure-viscosity coefficient α is 15.9 GPa^{-1}, the ambient viscosity η_0 is

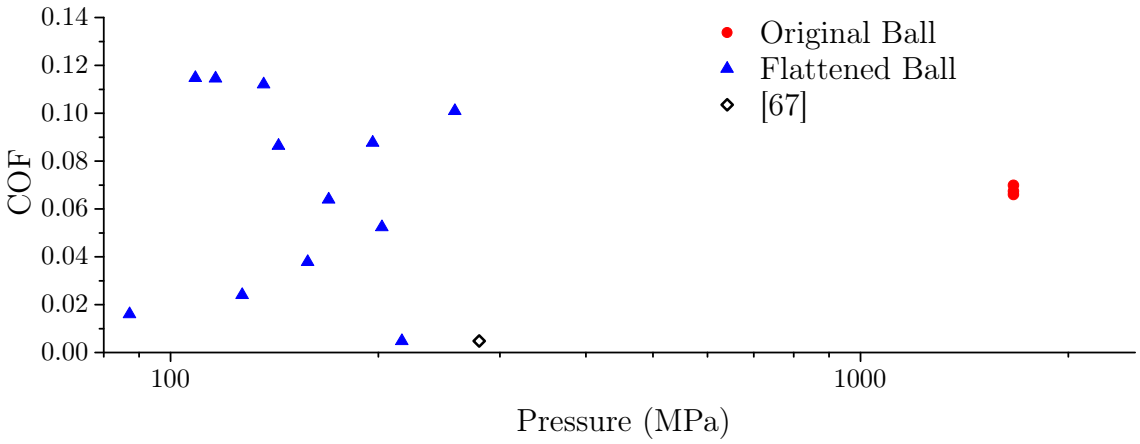

Figure 3.6: Friction as a function of pressure at constant speed (~ 31 mm/s) for the original and flattened balls. All tests were performed at a load of 30 N and the pressure varies due to the radius of the flattened ball. Also shown is the result obtained with a pin-on-flat geometry in [67] (hollow symbol).

0.674 Pa·s, the load F is 30 N, and the ellipticity parameter k is 1 for a spherical geometry. The film parameter λ was calculated for all twelve flattened ball cases and the results are shown in Figure 3.7. The friction decreased with increasing λ. The three tests with $\lambda \approx 1$, suggesting nearly boundary lubrication, corresponded to the roughest surfaces ($R_{a,ball} = 257.3 \pm 27.3$ nm). All other tests had a λ value of greater than 3, indicating full film lubrication. The test that exhibited ultra-low friction (friction coefficient < 0.01) corresponded to a surface roughness of 17.7 nm and $\lambda > 10$. Therefore, although the measured ultra-low friction is comparable to that reported in [67], here this result was only achieved with full film lubrication, i.e. not through the action of a protective tribofilm. Using the film thickness calculation described above, the film parameter for the data point at comparable speed reported in [67] is slightly below 1, indicating boundary lubrication. Therefore, the previously reported superlubricity could not be reproduced or explained. Possible explanations of the disparity include differing geometry and material composition, since the present NiTi was alloyed with Hafnium and the large radii were created artificially using severe wear of the balls. Additionally, another recent study by a different group measured friction with 60NiTi and 58Ni39Ti-3Hf lubricated by castor oil lubricated and found a COF of ≥ 0.1, much higher than the superlubricity limit [55].

3.4 Conclusion

The ability of castor oil to lubricate a NiTi-Hf / steel contacts was evaluated by measuring the friction coefficient in pure sliding conditions under a range of

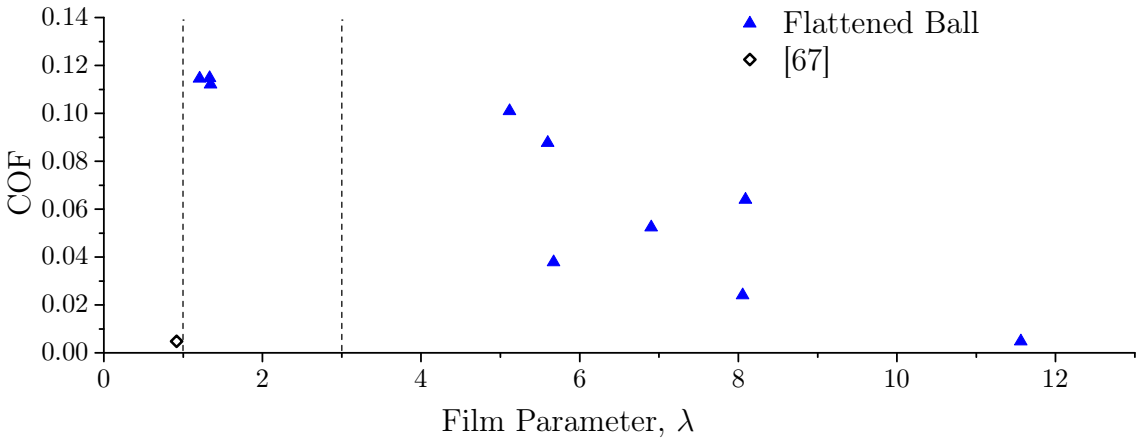

Figure 3.7: Friction as a function of the film parameter λ for the flattened ball tests at $\sim$31 mm/s. Also shown is the result obtained with a pin-on-flat geometry in [67] (hollow symbol). Vertical dashed lines indicate theoretical transitions between lubrication regimes.

speeds, pressures and surface roughness. With spherical NiTi-Hf balls, it was found that the effect of speed was consistent with that expected based on a traditional Stribeck curve. However, at all speeds, the observed friction was significantly higher than reported in [67]. To minimize differences between the two studies, the NiTi-Hf balls were subjected to controlled wear prior to friction testing in order to achieve lower pressures and geometries comparable to a pin-on-disk geometries. With these flattened balls, friction was still higher than previously-reported. The effect of pressure was explored for a given speed by testing with different flattened ball radii, and it was found that friction did not vary monotonically with pressure. However, measurements with different surface roughness revealed a strong dependence of friction. With the smoothest NiTi-Hf surfaces (Ra$\approx$18 nm), ultra-low friction was achieved. However, an analysis of the film parameter λ revealed that this case was likely to be in the full film lubrication regime, where low friction was provided by the fluid entirely supporting the load. Therefore, in contrast to findings of the previous study, it is unlikely that the ultra-low friction observed here was due to the effects of a tribofilm. Regardless, the present study shows that castor oil may be used to lubricate NiTi-Hf, but only if the components are finished to achieve small surface roughness and then maintain that roughness level during operation.

Chapter 4

EVALUATING SEVERAL GREASES FOR BOUNDARY LUBRICATION OF SELF-MATED 60NITI

4.1 Grease Lubrication for 60NiTi

60NiTi has many properties that are desirable for bearing materials, especially those used in space applications where components must operate efficiently and reliably in harsh conditions. However, despite the fact that most bearings are grease lubricated, there has not yet been a systematic study of the tribo-performance of greases for 60NiTi lubrication. To address this, five different greases were selected to evaluate their tribological performance in lubricating in low sliding speed self-mated NiTi-Hf contacts. The greases, their kinematic viscosities, base oil chemistry, and thicker chemistry are summarized in Table 4.1. Three of the greases used, (Braycote 601EF, Braycote 602EF and Nye Rheolube 2000), are designed for use in space/vacuum applications where low outgassing and low volatility are necessary. Nye Rheolube 374A and SKF LGMT2 are conventional mineral and synthetic oil greases used in both aviation and terrestrial applications. The base oil of Nye Rheolube 2000 is Pennzane 2001A and the base oil of Braycote 601EF and 602EF is Braycote 815z; Pennzane 2001A and Braycote 815z have been characterized in previous studies of self-mated NiTi-Hf in rolling-sliding contact [16, 20–22, 25].

Table 4.1: Tabulated summary of greases used in this study, and their properties.

Grease	Base Oil	Thickner type	Viscosity 40, 100 ℃
LGMT2	Mineral Oil	Lithium Soap	110, 11 cSt
Braycote 601EF	PFPE (Brayco 815Z)	PTFE Particles	148, 45 cSt
Braycote 602EF	PFPE (Brayco 815Z)	PTFE Particles	140, 45 cSt
Rheolube 374A	PAO	Lithium Soap	121, 17 cSt
Rheolube 2000	MAC (Pennzane 2001A)	Sodium Soap	110, 15 cSt

4.2 Testing Conditions

Tests were performed following an adaptation of the ASTM G133-05 standard for linear reciprocating ball-on-flat sliding wear tests in the configuration shown in

Figure 2.1(a), with modifications necessitated by limitations of the available test instrumentation. The ASTM standard recommends a 10 mm stroke length at 10 Hz oscillating frequency (200 mm/s sliding speed). However, the present tests were performed with a 10 mm stroke length, at 0.25 Hz oscillating frequency (5 mm/s sliding speed). The samples were polished to an R_a of 46 nm and 6 nm for the ball and flat respectively, as measured by a white light interferometer. The load was chosen to be close, but still comfortably less than the allowable contact stress for bearing materials in high precision mechanisms listed in NASA standard no. 5017A [74]. For each grease, three tests were run with a 30 m sliding distance and one test with a 100 m sliding distance. Prior to each test, each sample was ultrasonically cleaned in a heptane bath, and again in Vertrel XF ifz fluorinated oil was present. For each test, approximately 0.5 g of grease was evenly spread along the path of the ball. The test conditions are summarized in Table 4.2.

Table 4.2: Test parameters used for ASTM G133-05 reciprocating tests.

Parameter	Value
Stroke Length	10 m
Sliding Speed	5 mms^{-1}
Sliding Distance	30, 100 m
Contact Pressure	~ 1 GPa
Ball Diameter	3/16"
Surface Roughness	Ball - 46 nm
	Flat - 4 nm
Lubricant	Grease
Humidity	35–50%
Trials	3

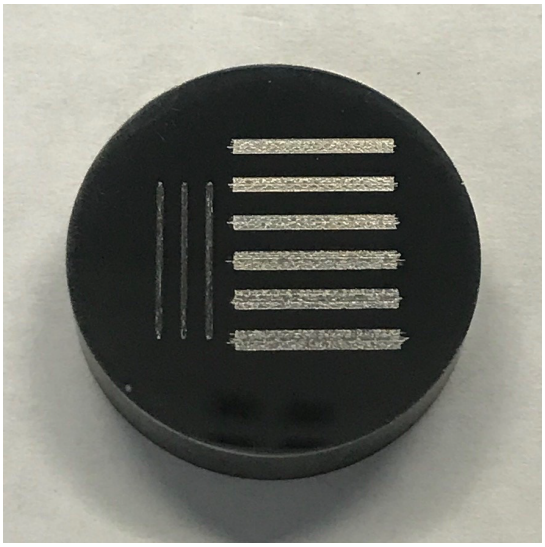

Figure 4.1: Polished NiTi-Hf sample with wear tracks from wear testing.

For each grease, the friction and wear behavior is analyzed. First, the COF is shown as a function of sliding distance for four tests (three at 30 m and one at 100 m). The friction traces of the three 30 m tests are shown as red, black, and blue, and the 100 m tests are shown in magenta. Then, representative wear scars from the ball and the flat are shown from one 30 m test for each grease. Wear was evaluated using optical and interferometer images, SEM images within the wear scar on the flat, wear volume (calculated per Sections 2.3 and 2.4). Optical images were taken using a Leica (Model DM 2500M) optical microscope, and SEM images by Zeiss Gemini 500 scanning electron microscope. Prior to imaging, each surface was thoroughly cleaned using the same procedure as was used prior to testing.

4.3 SKF LGMT Results

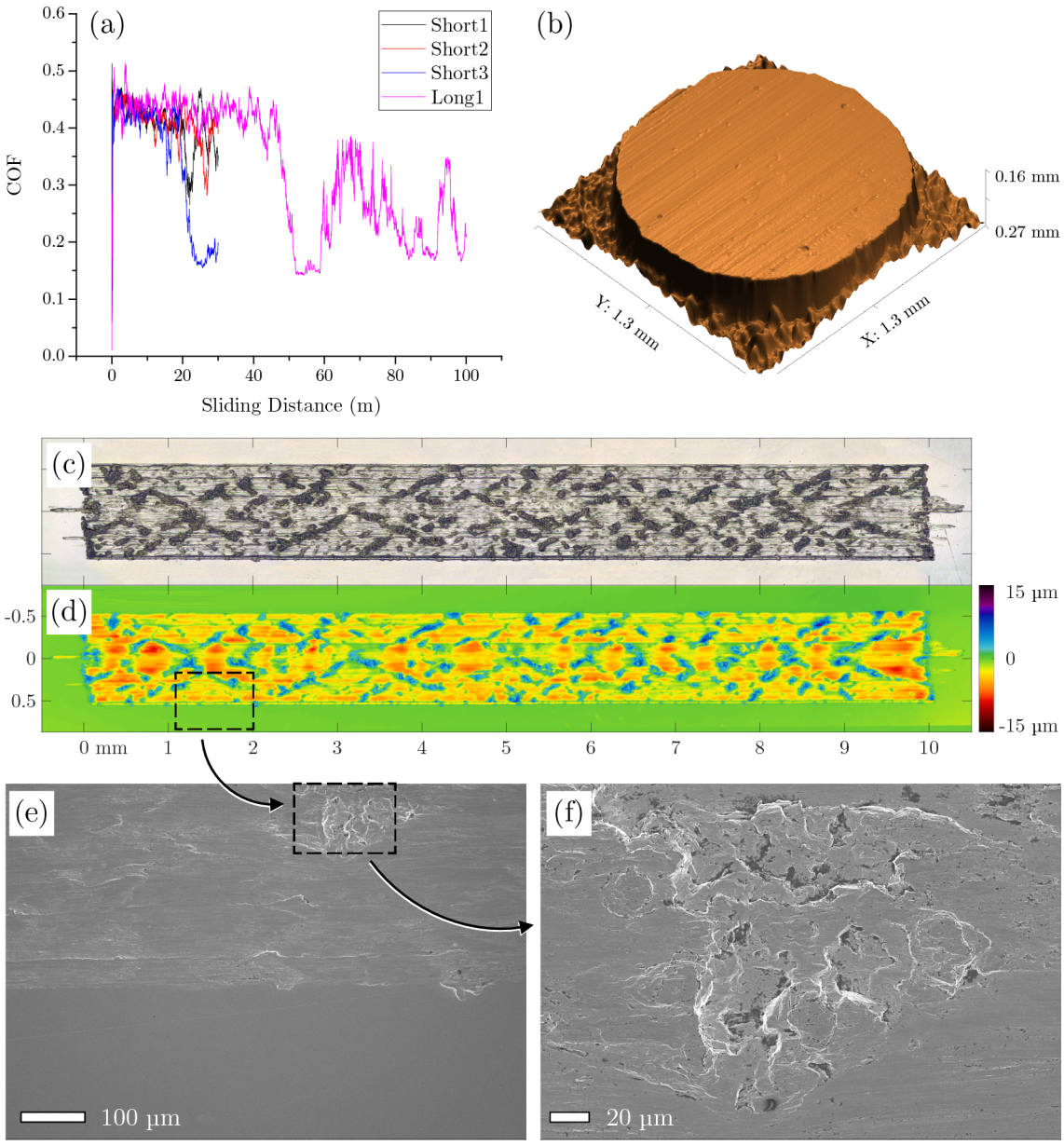

Figure 4.2: Test results for SKF LGMT2 including (a) friction traces, (b) interferometer image of the ball wear scar, (c) and (d) optical microscope and interferometer images of the flat wear scar, and (e) and (f) SEM micrographs of the flat wear scar. All wear images correspond to the test shown in blue in (a)

Test results for the SKF LGMT2 are shown in Figure 4.2. The COF, shown in Figure 4.2(a), is initially high (~ 0.45). In one of the 30 m trials, the friction starts

to decrease around 20 m of sliding. This decrease also happens in the 100 m test at 40 m of sliding. However, the friction is never observed to be consistently low with this grease. Figure 4.2(b) shows the wear scar on the ball with severe scoring marks parallel to the sliding direction, indicating predominantly abrasive wear [10, 70]. The corresponding scar on the flat shows faint abrasive wear marks and protruding features which are indicated by the blue regions in the interferometer image in Figure 4.2(c) and dark regions in the optical microscope image in Figure 4.2(d). These protruding features are likely adhered wear debris. Two regions are magnified in SEM micrographs in Figures 4.2(e) and 4.2(f) which show that the size of the adhered features ranges from a few tens to hundreds of microns, indicating this behavior is prevalent across different scales of asperity contact. The large amount of material adhesion is possibly a result of galling [70], which would be consistent with the behavior of other titanium rich alloys [20,21,56] in sliding. A $\times$20 magnification

Figure 4.3: $\times$20 Optical microscope image of one protruding feature taken inside the LGMT wear track shown in Figure 4.2(c)

optical microscope image shown in Figure 4.8 details one protruding feature as well as the deep abrasive marks in the direction of sliding. This indicates that adhesive wear on the flat is still highly prevalent despite the large amount of adhered material. It is possible that wear debris adheres to the flat and is work-hardened due to the severe testing conditions and then the hard protruding material on the flat abrades the relatively softer ball.

4.4 Braycote 601EF Results

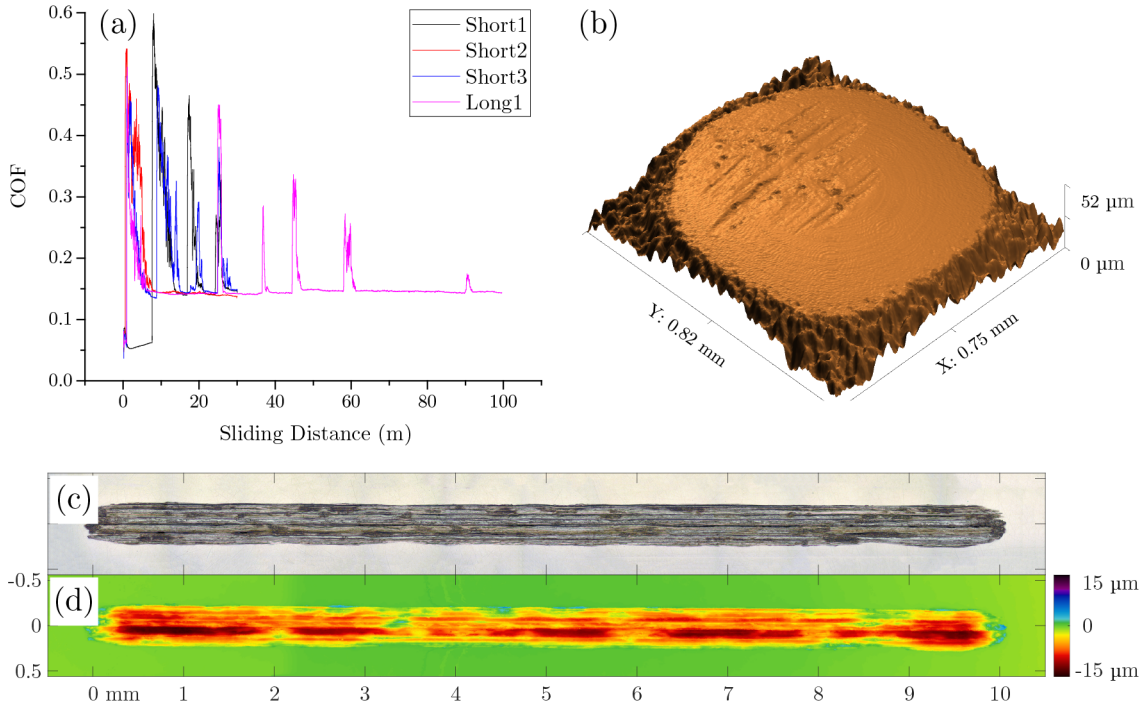

Figure 4.4: Test results for Braycote 601EF including (a) friction traces, (b) interferometer image of the ball wear scar, (d) interferometer image of the flat wear scar, and (c) optical image of the flat wear scar. All wear images correspond to the test shown in blue in (a)

Test results for Braycote 601EF are shown in Figure 4.4. The COF, shown in Figure 4.4(a) was consistent between all four tests. For each test, there was a short run in period followed by low friction (average COF of 0.14 after 10 m of sliding) with intermittent friction peaks, possibly due to wear followed by removal of worn material from the wear track. The longer duration test (100 m sliding distance) shows that the height and frequency of these friction peaks decrease with sliding distance. Ball wear, shown in Figure 4.4(b), was very relatively smaller than in tests with other greases. Unlike the the SKF LGMT2 tests, there are no protruding features found on the flat wear scar shown in Figures 4.4(c) and 4.4(d), which suggests this contact is dominated by abrasive wear [10] as evidenced by the longitudinal grooves in Figure 4.4(d). While the width of the wear scar on the flat is much smaller than that with the SKF LGMT2 shown in Figure 4.2(d), the wear depth is much greater. Which is shown by the larger and darker regions of red in Figure 4.2(d). The lack of protruding features may indicate that the PTFE particles, that thicken Braycote 601, are effective at preventing adhesive wear modes.

4.5 Bracycote 602EF Results

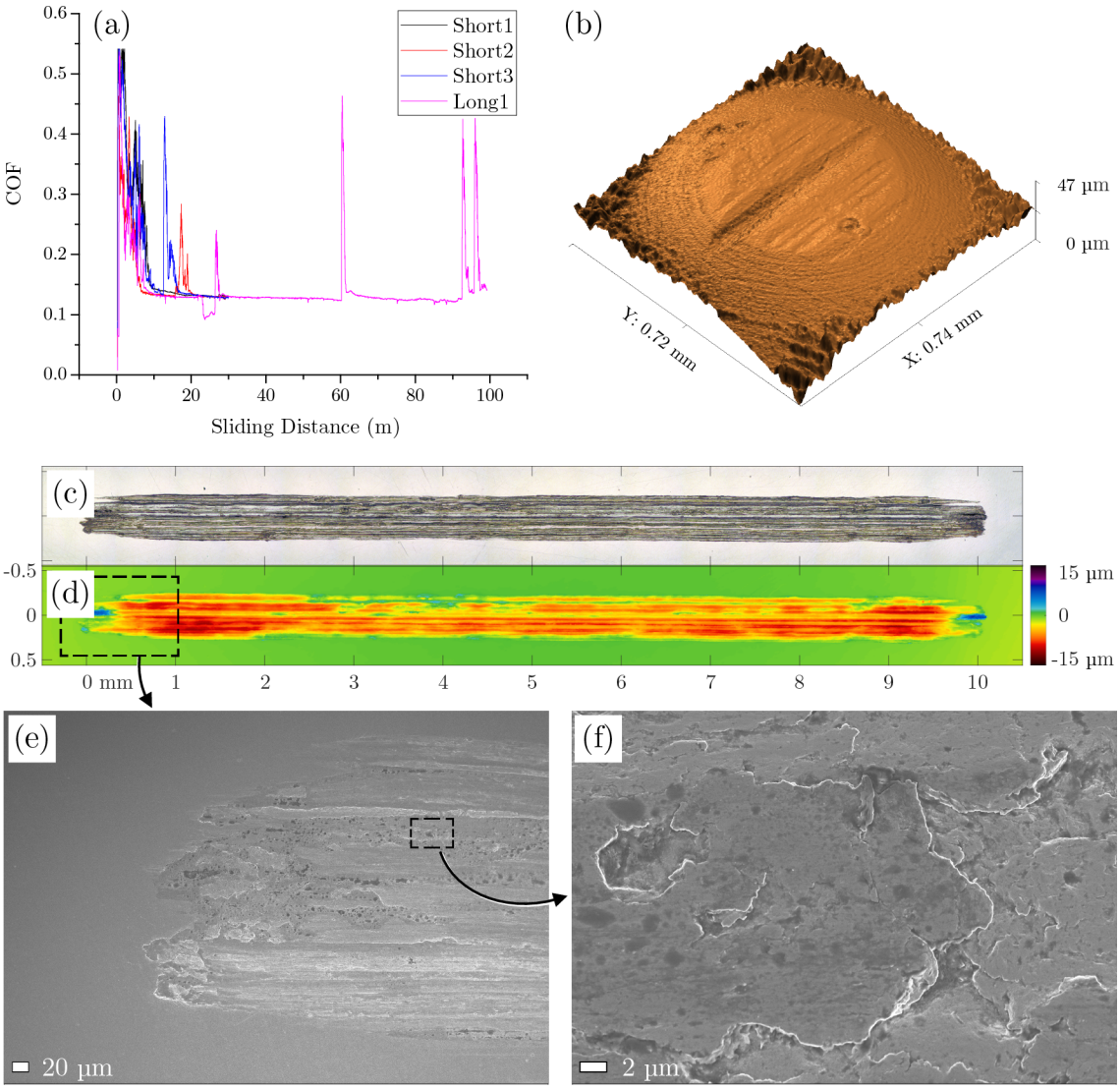

Figure 4.5: Test results for Braycote 602EF including (a) friction traces, (b) interferometer image of the ball wear scar, (c) and (d) optical microscope and interferometer images of the flat wear scar, and (e) and (f) SEM micrographs of the flat wear scar. All wear images correspond to the test shown in blue in (a)

Test results for Braycote 602EF are shown in Figure 4.5. The COF, shown in Figure 4.4(a) are similar to those from the Braycote 601EF, but with fewer friction peaks. The mean COF after 10 m of sliding is slightly lower at 0.13, which is possibly due to the addition of 2 w.t.% MoS_2 which is intended to help reduce friction

in boundary lubrication. The wear on the ball shown in Figure 4.5(b), and flat in Figures 4.5(c) and 4.5(d) are also similar to those of Braycote 601EF, characterized by narrow, sometimes deep wear features, indicating abrasive wear. SEM micrographs of the flat wear scar for this grease contain many micron-sized dark spots, as shown in Figures 4.5(e) and 4.5(f). Since the SEM was performed after the sample was ultrasonically cleaned in a bath of Vertrel XF for 5 mintues and dried with forced air, it is unlikely these are residual spots of grease. Additionally, similar spots were observed with the Braycote 601EF, but a significantly lower superficial density compared to Braycote 602EF. Compositional analysis using energy-dispersive x-ray spectroscopy (EDAX) was performed on these scars to investigate the dark spots, and the spectrum for one spot in the wear track shown in Figures 4.5(c) to 4.5(f) is shown in Figure 4.6. The EDS spectrum show peaks for nickel, titanium, and

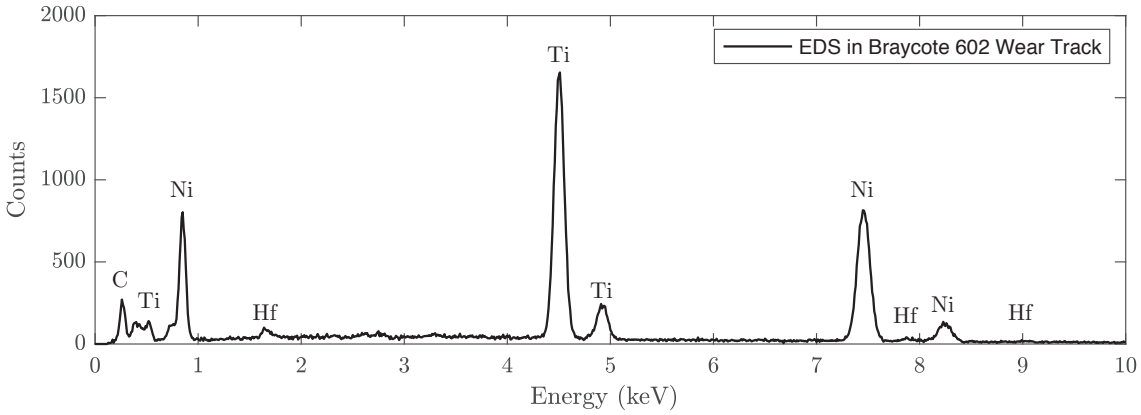

Figure 4.6: EDS spectrum of NiTi-Hf wear track in the wear track created during one Braycote 602EF lubricated test.

hafnium where expected. There were very few counts in the range that would be expected for molybdenum or sulfur, so the dark spots shown in Figure 4.5(f) are not explained by residual MoS_2. There is a small peak for carbon which may indicate some residual tribochemical product as the organic lubricant is degraded. Since the spots are so scarce and the the typical detection limit for EDS performed by an SEM is ~ 0.1 wt%, it is possible that there is something unaccounted for here, present at levels below that detectable threshold. So overall these EDS measurements do not conclusively explain the nature of the observed dark spots in Figure 4.5(f).

4.6 Nye Rheolube 374A Results

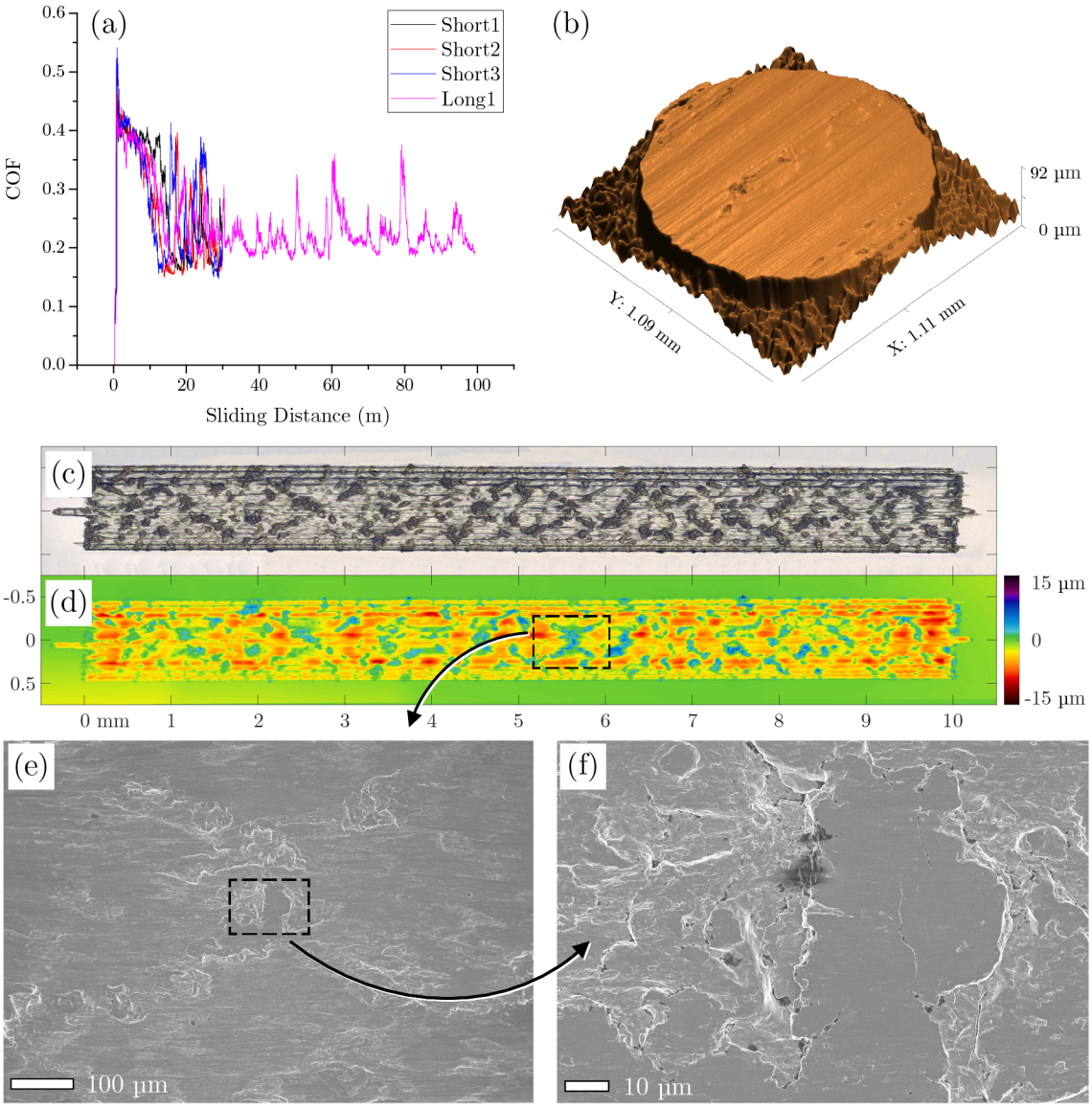

Figure 4.7: Test results for Rheolube 374A including (a) friction traces, (b) interferometer image of the ball wear scar, (c) and (d) optical microscope and interferometer images of the flat wear scar, and (e) and (f) SEM micrographs of the flat wear scar. All wear images correspond to the test shown in red in (a)

Test results with Rheolube 374A are shown in Figure 4.7. The COF, shown in Figure 4.7(a) decreases in the first 7 m of sliding, after which the friction is erratic

and relatively high (average friction of 0.22 as calculated after 15 m of sliding). This behavior is similar to that of SKF LGMT2, but the friction decreases with sliding distance more quickly with the Rheolube 374A. The longer duration test exhibits the same trends as those run for 30 m, with a rapid friction decrease leading to erratic friction with an average value of 0.22 after 15 m. The interferometer image of the ball wear scar in Figure 4.7(b) shows significant wear and abrasive wear marks, similar to the SKF LGMT2. Also, the wear scars shown in Figures 4.7(c) and 4.7(d) suggest a combination of adhesive and abrasive wear, as evidenced by protruding features that are higher than the original surface (blue in the interferometer image) and abrasive scoring marks (yellow streaks). While the mechanisms appear to be similar

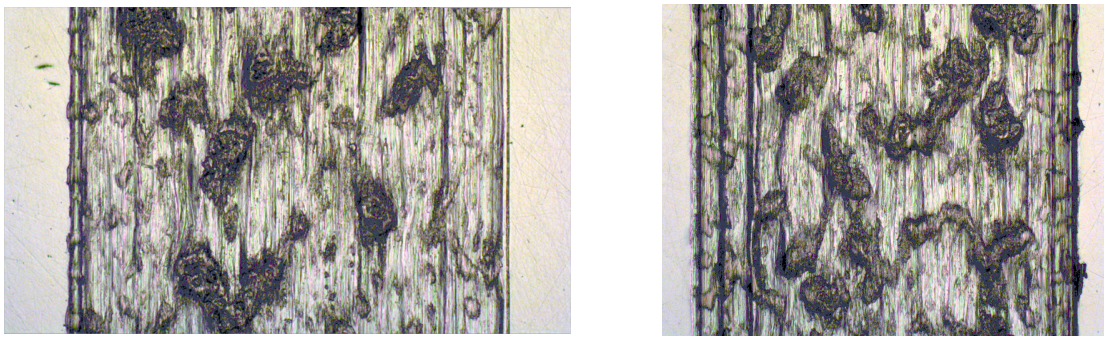

Figure 4.8: Representative sections from the optical microscope images of the wear track for (a) LGMT and (b) 374A.

to what was observed in the SKF LGMT2 wear track, Rheolube 374A had smaller wear tracks with much higher superficial density of protruding features as shown in Figure 4.8. Additionally, the protruding features in 374A were shorter relative to the surface compared to features observed in the LGMT tests. SEM micrographs of the protruding features from the wear scar are shown in Figures 4.7(e) and 4.7(f) suggest that the material adhered to the flat has been sheared and flattened due to cyclic shear stresses.

4.7 Nye Rheolube 2000 Results

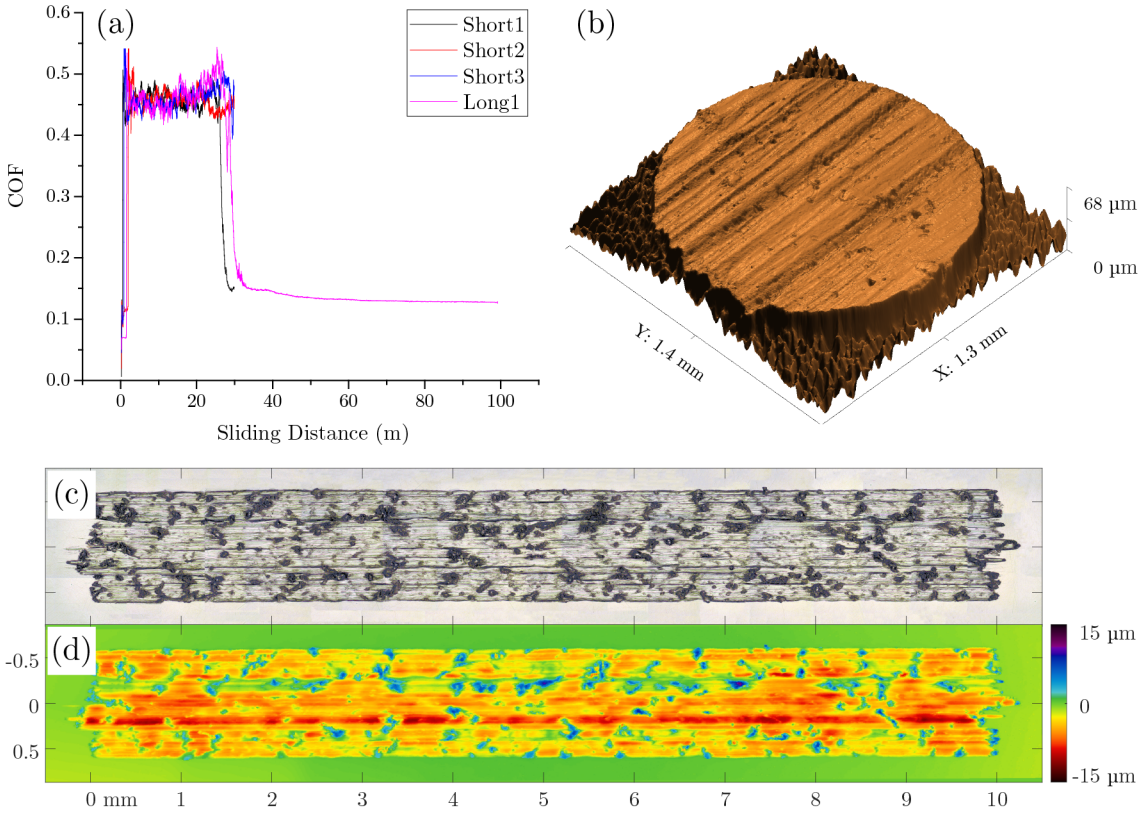

Figure 4.9: Test results for Rherolube 200 including (a) friction traces, (b) interferometer image of the ball wear scar, and (c) and (d) optical microscope and interferometer images of the flat wear scar. All wear images correspond to the test shown in blue in (a)

Test results with the Rheolube 2000 are shown in Figure 4.9. The COF, shown in Figure 4.9(a) stays between 0.4 and 0.5 until 25 to 30 m of sliding, after which it drops to a constant value of 0.13. The interferometer image of the ball wear scar in Figure 4.9(b) shows severe abrasive wear, similar to that observed with Rheolube 374A and SKF LGMT2. The Rheolube 2000 ball wear scar differs, however, in that it exhibits micro-sized pits along with the scoring marks. The flat wear scar width and appearance resemble the Rheolube 374A with protruding features and mild abrasive scoring marks. However, unlike the Rheolube 374A and SKF LGMT2, here the presence of adhered material inside flat wear scar and severe abrasion on ball did not result in high, erratic friction in the 100 m test. This is possibly due to increased contact area (inferred from the relatively larger wear scar) which would result in a lower contact stress.

4.8 Conclusion

Table 4.3: Specific wear rates ($\times 10^{-5}$ mm^3/m·N) calculated from the 30 m tests.

Grease	Flat	Ball	Combined
LGMT2	6.3 ± 1.1	14.4 ± 1.7	20.7 ± 2.0
Braycote 601EF	5.4 ± 0.7	0.2 ± 0.1	5.6 ± 0.7
Braycote 602EF	5.7 ± 1.2	0.3 ± 0.1	5.9 ± 1.2
Rheolube 374A	6.2 ± 0.7	4.9 ± 0.4	11.1 ± 0.8
Rheolube 2000	10.5 ± 0.9	15.8 ± 0.7	26.3 ± 1.1

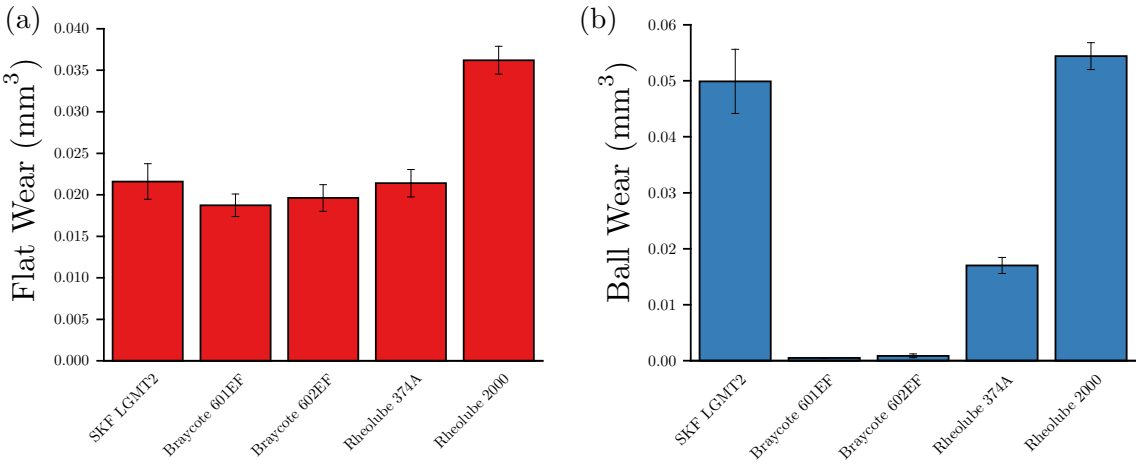

Figure 4.10: Wear volume averaged over the three 30 m tests for each grease as measured from the (a) flat and (b) ball. Error bars represent the standard error of three tests.

To compare the wear behavior of each grease quantitatively, the wear volume on the ball and flat was calculated from the 3D interferometer images of the wear scars as described in Sections 2.3 and 2.4. Specific wear rates were calculated for the three short sliding distances as the wear volume divided by the total sliding distance (30 m) and normal load (11.5 N). The results are shown in Figure 4.10. The wear volume comparison shows that flat wear (Figure 4.10(a)) is nearly the same in all cases, except for Rheolube 2000 which has nearly twice the wear of the other greases. However, the similarity in the wear volume is misleading since the SKF LGMT2 and Rheolube 374A wear tracks are wide with significant adhered material, while the flat wear scars of the two Braycote greases are narrower and deeper as demonstrated in Figure 4.11. However, the difference in overall wear performance is more obvious

in the comparison of ball wear, shown in Figure 4.10(b). The two Braycote greases have an order of magnitude lower wear than the other greases. This is followed by the Rheolube 374A, and then the SKF LGMT2 and Rheolube 374A that have the most ball wear. For SKF LGMT2 and Rheolube 374A, the ball wear is greater than that of the flat, likely due to material that adheres to the flat during testing.

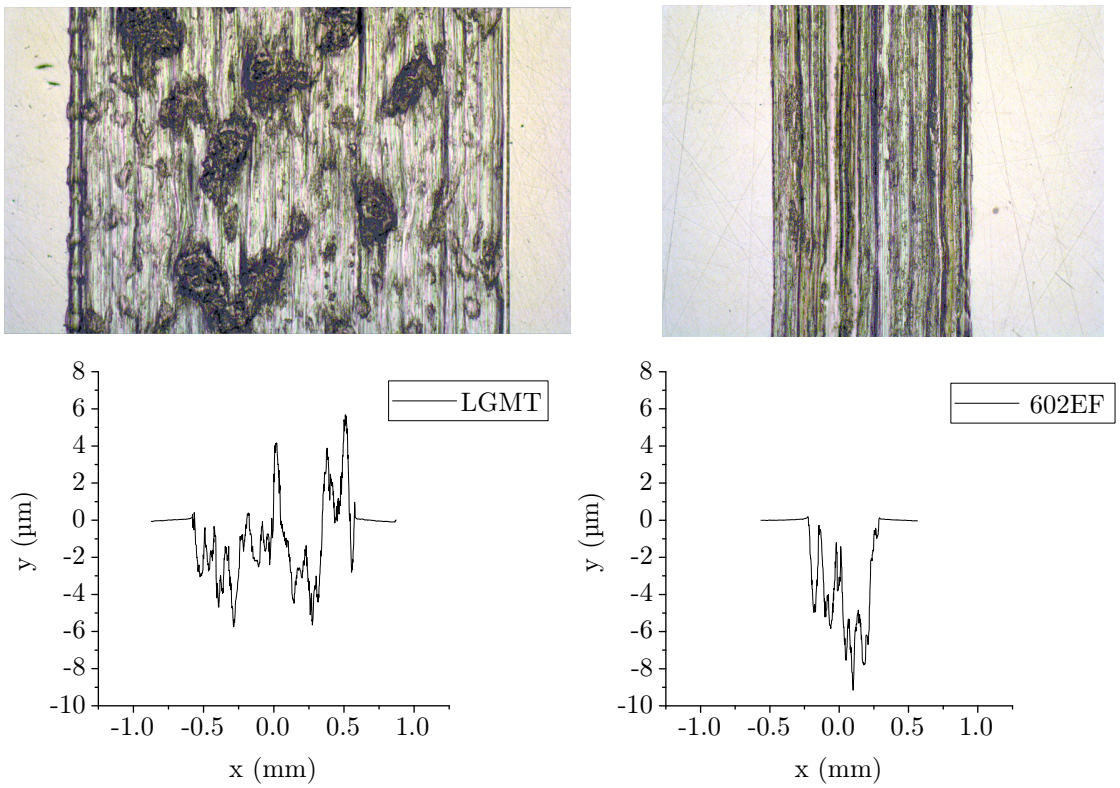

Figure 4.11: Representative sections from the optical microscope images of the wear track for (a) LGMT and (b) Braycote 602EF and representative cross sectional profiles for (c) LGMT and (d) Braycote 602 EF.

The specific wear rates with each grease for the ball, the flat and for both surfaces from the 30 m tests are summarized in Table 4.3. The trends in specific wear rate for the ball and flat reflect the trends observed in Figure 4.10. It should be noted that the flat wear rates in the present tests are comparable to those reported in other studies with NiTi-Hf sliding against tungsten carbide ball with castor oil or fully-formulated PAO gear oil [55, 57, 58]. The combined wear rates enable direct comparison of the greases and show that, in terms of wear resistance, the greases tested here compare as follows: Nye Rheolube 2000 $<$ SKF LGMT2 $<$ Nye Rheolube 374A $<$ Braycote 602EF $\approx$ Braycote 601EF.

The results from this study can be analyzed in the context of previous reports of NiTi-Hf tribo-performance. First, the Rheolube 2000 tests can be compared to spiral orbit tribometer measurements of self-mated 60NiTi using Pennzane 2001A oil lubrication [16], which is the base fluid in Rheolube 2000. Unlike the results shown in Figure 4.9, the previous study reported that 60NiTi is amenable to lubrication with Pennzane 2001A and rolling-sliding contact was measured with a low, steady COF of approximately 0.06 and no material adhesion. The Hertz contact pressure was ~ 1 GPa in both studies, so the differences are likely due to the severity of the test conditions, i.e. the present tests are pure sliding which is much more severe than rolling-sliding contact. Another comparison can be made related to the adhered material features we observed in the flat wear tracks for SKF LGMT2, Rheolube 374A and Rheolube 2000. These features are similar to those found in the flat wear tracks after sliding a tungsten carbide ball on NiTi-Hf in unlubricated conditions at similar contact pressures [58], which may be adhered wear debris.

The composition of the protruding features was measured using energy dispersive x-ray spectroscopy and showed that the material mainly consisted of Nickel, Titanium, Oxygen, and a negligibly small amount of ball material, which suggested that the protruding features did not form due to material transfer from ball to flat. In the present study of self-mated NiTi-Hf, it is likely that the protruding features consist of material that was originally from both the ball and the flat. However, no such features were observed in the rolling-sliding spiral orbit tribometer tests for self-mated 60NiTi lubricated with Pennzane 2001A oil in [16]. These observations suggest that the protruding features observed in this study may have formed while the ball was sliding against the flat in starved lubrication conditions. It is known that grease lubricated contacts are susceptible to starved lubrication conditions when the grease is unable to supply the contact with a sufficient amount of oil [75, 76], which would explain the similarity between our tests and the unlubricated tests from [58].

The goal of this study was to evaluate the tribo-performance of self-mated NiTi-Hf under grease lubrication. Five greases were tested, including those currently used in space and terrestrial applications: a mineral-oil-based general purpose grease (SKF LGMT2), a PFPE-based grease (Braycote 601EF) and additized with MoS_2 (Braycote 602EF), a PAO-based high temperature grease (Rheolube 374A) and a MAC-based grease (Rheolube 2000). The performance of these greases was evaluated for pure sliding at 1 GPa in a non-conformal contact. This emulates severe conditions that correspond to contacts that are lubricant-starved and cease rolling. The greases are compared in terms of friction as well as wear measured using an optical microscope, interferometer and SEM imaging of the wear scars on the ball and flat. The observations for each grease are summarized below:

1. SKF LGMT2 exhibited high friction, with a COF in the range of 0.15 to 0.4, even after run-in. The wear on ball was high and almost twice that of the wear

on the flat. A significant amount of material adhered to the flat, extending above the original surface height. The wear patterns on the ball and flat suggest that both adhesive and abrasive wear mechanisms are present.

2. Braycote 601EF and Braycote 602EF exhibited low CoFs of 0.14 and 0.13, respectively, with intermittent friction-peaks, likely due to wear followed by wear debris removal from the contact. Fewer and smaller friction peaks were observed with the Braycote 602EF possibly due to the addition of MoS_2. In both cases, the ball wear was minimal. The flat wear tracks, although narrower than observed with the other three greases, were deeper and did not contain protruding features, which indicates predominantly abrasive wear. The flat wear track with the Braycote 602EF exhibited dark spots in SEM micrographs, the origin of which are not clear.

3. Rheolube 374 showed friction that began to decrease quickly (within 17 m), but then entered varied erratically for the rest of the test duration with high COFs between 0.2 and 0.3. Wear on the ball was significantly lower than with the SKF LGMT2, but higher than with the Braycote greases. Wear on the flat suggested a combination of abrasive and adhesive wear mechanisms.

4. Rheolube 2000 exhibited high friction (COF between 0.4 and 0.5) until ~ 30 m, after which the friction dropped dramatically to an average of 0.13 and remained steady until the end of the long test. Wear was the highest with this grease on both the ball and flat. Protruding features were observed, similar to SKF LGMT2 and Rheolube 374, but in this case their presence did not adversely affect the friction after run-in.

Overall, both the PFPE based and PTFE thickened greases (Braycote 601 and 602 EF) performed the best, with the lowest friction and best wear resistance. Of those two, the 602EF exhibited slightly lower average friction and wear, possibly due to the presence of the MoS_2 additive, but the difference was not statistically significant. Compared to the other three greases, the mineral-oil-based general purpose grease (SKF LGMT2) and MAC-based grease (Rheolube 2000) performed the worst, exhibiting high friction throughout the test and significant wear. The PAO-based high temperature grease (Rheolube 374A) was moderate in both friction and wear. The results of this study are the first step towards a complete evaluation of the friction and wear performance of self-mated NiTi-Hf contacts.

Chapter 5

FUTURE RESEARCH

5.1 Mitigating Wear in 60NiTi Self Mated Contacts

60NiTi has shown a tendency to experience significant adhesive wear under certain conditions. Further work should investigate the mechanism of this wear behavior, and techniques to mitigate it. This may include investigations into surface treatments or solid film coatings that will be effective at minimizing adhesive wear. Here, it was proposed that work hardened wear debris caused aggravated wear, but [68] showed that controlled work hardening could provide improved wear resistance. Future studies should investigate techniques of either mitigating or controlling the work hardening of the surface of 60NiTi to enable better tribological performance. Most studies performed so far have been sliding ball-on-disk tests. However, components made from 60NiTi, such as bearings and gears, will experience rolling-sliding contacts. Future investigations of 60NiTi should include rolling-sliding contacts and different loading conditions than presented here. Only with a comprehensive set of data for performance of 60NiTi under different conditions, will the use of this material for greater and wider wider variety of potential bearing applications be enabled.

5.2 Hybrid NiTi-Hf Counterface Mechanisms

Titanium rich alloys are prone to adhesive wear in self mated contacts, so sliding against an unlike counterface material could enable enhanced performance and component life. For example, other titanium alloys such as aluminum-titanium show better wear performance sliding against 440C than they do in self mated contacts [77]. NASA Glenn also envisions applications with both hybrid Si_3N_4/NiTi-Hf and hybrid 440C/NiTi-Hf bearings [44]. There has been work done to characterize 60NiTi in dissimilar contacts [54, 57, 58, 65–67]. However, more study is still required to understand how to lubricate those dissimilar contacts and to select potentially more advantageous counterface materials. Specifically, additional studies of Si_3N_4/NiTi-Hf and 440C/NiTi-Hf contacts should be conducted to inform design considerations for hybrid bearings.

5.3 Lubricant Chemistries

There have been decades of research and development done to design lubricants to function through chemical and physical interactions with steel surfaces. Comparatively, much less work has been done to investigate possible additive chemistires for titanium alloys. In the 1960's, early studies of the tribological properties of titanium suggested the use of charge transfer complex of iodine and aromatic compounds (like n-Butylbenzene) as an oil additives for titanium and titanium rich alloys [78–80]. These studies reported significant reduction in friction and wear with the use of these compounds as oil additives. Future research should explore the use of nontraditional oil additives for 60NiTi.

5.4 Concluding Remarks

60NiTi shows remarkable potential for the application of highly resilient components for mechanical systems. With more research and development, intermetallic alloys are poised to join ceramics and martensitic steels as well recognized bearing materials. Additionally, as Chris Dellacorte remarks in [20], our strong understanding of the Fe-C system only developed as the result of many decades of research. The Ni-Ti system has only just begun to be explored and has the potential to reveal new and exciting properties we have not yet observed.

BIBLIOGRAPHY

[1] Liddell, H. G. and Scott, R., 1889, *An Intermediate Greek-English Lexicon*, Oxford, Clarendon Press.

[2] Jost, H. P. and Great Britain. Department of Education and Science. Lubrication Engineering (Education and Research) Working Group., 1966, "Lubrication (Tribology), Education and Research; A Report on the Present Position and Industry's Needs." 6s. 6d. ne, Great Britain Department of Education and Science, London.

[3] Dowson, D., 1998, *History of Tribology*, Professional Engineering Pub.

[4] Fitch, J., 2006, "Interview with Luminary Professor H. Peter Jost - The Man Who Gave Birth to the Word 'Tribology'," Machinery Lubrication.

[5] Holmberg, K. and Erdemir, A., 2017, "Influence of Tribology on Global Energy Consumption, Costs and Emissions," Friction, **5**(3), pp. 263–284, doi: 10.1007/s40544-017-0183-5.

[6] Lee, P., Carpick, R., Jackson, A., Argibay, N., Pachon Garcia, A., Sawyer, W., and Bennet, K., 2017, "Tribological Opportunities for Enhancing America's Energy Efficiency. A Report to the Advanced Research Projects Agency-Energy (ARPA-E) at the U.S. Department of Energy," , U.S. Department of Energy.

[7] Jost, H. P., 2005, "Tribology Micro & Macro Economics: A Road to Economic Savings," Tribology and Lubrication Technology, **61**(10), pp. 18–23.

[8] Baykara, M. Z., Vazirisereshk, M. R., and Martini, A., 2018, "Emerging Superlubricity: A Review of the State of the Art and Perspectives on Future Research," Applied Physics Reviews, **5**(4), p. 041102, doi: 10.1063/1.5051445.

[9] Popov, V. L., 2018, "Is Tribology Approaching Its Golden Age? Grand Challenges in Engineering Education and Tribological Research," Frontiers in Mechanical Engineering, **4**, p. 16, doi: 10.3389/fmech.2018.00016.

[10] Bhushan, B., 2013, "Adhesion," *Introduction to Tribology*, John Wiley & Sons, Ltd, pp. 157–198, doi: 10.1002/9781118403259.ch4.

[11] Hsueh, C.-H. and Miranda, P., 2004, "Combined Empirical–Analytical Method for Determining Contact Radius and Indenter Displacement during Hertzian Indentation on Coating/Substrate Systems," Journal of Materials Research, **19**(9), pp. 2774–2781, doi: 10.1557/JMR.2004.0359.

[12] Hsueh, C.-H. and Miranda, P., 2004, "Master Curves for Hertzian Indentation on Coating/Substrate Systems," Journal of Materials Research, **19**(1), pp. 94–100, doi: 10.1557/jmr.2004.19.1.94.

[13] Hamrock, B. J., Schmid, S. R., Jacobson, B. O., Schmid, S. R., and Jacobson, B. O., 2004, *Fundamentals of Fluid Film Lubrication*, CRC Press, doi: 10.1201/9780203021187.

[14] Davim, J. P., ed., 2011, *Tribology for Engineers: A Practical Guide*, 1st ed., Woodhead Publishing, Cambridge, UK, doi: 10.1533/9780857091444.65.

[15] Stachowiak, G. W. and Batchelor, A. W., 2014, "Chapter 7 - Elastohydrodynamic Lubrication," *Engineering Tribology (Fourth Edition)*, Butterworth-Heinemann, Boston, pp. 293–370, doi: 10.1016/B978-0-12-397047-3.00007-2.

[16] DellaCorte, C., 2010, "Nickel-Titanium Alloys: Corrosion "Proof" Alloys for Space Bearing, Components and Mechanism Applications," *Proceedings of the 40th*, Cocoa Beach, FL, pp. 293–300, NASA/CP-2010-216272.

[17] Buehler, W. J., Gilfrich, J. V., and Wiley, R. C., 1963, "Effect of Low-Temperature Phase Changes on the Mechanical Properties of Alloys near Composition TiNi," Journal of Applied Physics, **34**(5), pp. 1475–1477, doi: 10.1063/1.1729603.

[18] Buehler, W. J., May 14, 15, 16, 1963, "Intermetallic Compound Based Materials for Structural Applications," *The Seventh Navy Science Symposium: Solution to Navy Problems Through Advanced Technology* (Vol. 1), Office of Naval Research, U.S. Naval Aviation Medical Center, Pensacola, Florida., p. 1.

[19] Buehler, W. J., 2006, "NITINOL Re-Examination," White Oak Laboratory Alumni Association Leaf, **VIII**(I).

[20] DellaCorte, C. P., 2009, "Intermetallic Nickel-Titanium Alloys for Oil-Lubricated Bearing Applications," NASA/TM-2009-215646.

[21] Pepper, S. V., DellaCorte, C., Noebe, R. D., Hall, D. R., and Glennon, G., 2009, "Nitinol 60 as a Material For Spacecraft Triboelements," *13th European Space Mechanisms and Tribology Symposium*, Vienna, Austria, pp. 23–25.

[22] Pepper, S. V., Dellacorte, C., and Glennon, G., 2010, "Lubrication of Nitinol 60," NASA/TM-2010-216331.

[23] Stott, A. C., Brauer, J. I., Garg, A., Pepper, S. V., Abel, P. B., DellaCorte, C., Noebe, R. D., Glennon, G., Bylaska, E., and Dixon, D. A., 2010, "Bonding and Microstructural Stability in Ni 55 Ti 45 Studied by Experimental and Theoretical Methods," The Journal of Physical Chemistry C, **114**(46), pp. 19704–19713, doi: 10.1021/jp103552s.

[24] Stott, A. C., Abel, P. B., DellaCorte, C., Pepper, S. V., and Dixon, D. A., 2011/ed, "Computational Studies of the NiTi Alloy System: Bulk, Supercell, and Surface Calculations," MRS Online Proceedings Library Archive, **1295**, doi: 10.1557/opl.2011.556.

[25] DellaCorte, C., Noebe, R. D., Stanford, M. K., and Padula, S. A., 2012, "Resilient and Corrosion-Proof Rolling Element Bearings Made from Superelastic Ni-Ti Alloys for Aerospace Mechanism Applications," doi: 10.1520/STP103887, NASA/TM-2011-217105.

[26] DellaCorte, C. and Wozniak, W. A., 2012, "Design and Manufacturing Considerations for Shockproof and Corrosion-Immune Superelastic Nickel-Titanium Bearings for a Space Station Application," NASA/TM-2012-216015.

[27] DellaCorte, C., Moore, L. E., III, and Clifton, J. S., 2012, "Static Indentation Load Capacity of the Superelastic 60NiTi for Rolling Element Bearings," *2012 Annual Meeting and Exhibition Sponsored by the Society of Tribologists and Lubrication Engineers*, St. Louis, Missouri, p. 16, NASA/TM-2012-216016.

[28] Stanford, M. K., Thomas, F., and DellaCorte, C., 2012, "Processing Issues for Preliminary Melts of the Intermetallic Compound 60-NITINOL," .

[29] Stanford, M. K., Wozniak, W. A., and McCue, T. R., 2012, "Addressing Machining Issues for the Intermetallic Compound 60-NITINOL," NASA/TM-2012-216027.

[30] Stanford, M. K., 2012, "Thermophysical Properties of 60-NITINOL for Mechanical Component Applications," NASA/TM-2012-216056.

[31] Stanford, M. K., 2012, "Charpy Impact Energy and Microindentation Hardness of 60-NITINOL," NASA/TM-2012-216029.

[32] Stanford, M. K., Thomas, F., and Dellacorte, C., 2012, "Promoted-Ignition Testing to Determine the Gaseous Oxygen Compatibility of the Intermetallic Compound 60-NITINOL," NASA/TM-2012-216028.

[33] DellaCorte, C., Moore, L. E., III, and Clifton, J. S., 2013, "The Effect of Pre-Stressing on the Static Indentation Load Capacity of the Superelastic 60NiTi," NASA/TM—2013-216479.

[34] Dellacorte, C., 2014, "Novel Super-Elastic Materials for Advanced Bearing Applications," *13th 2014 CIMTEC International Ceramics Conference*, Florence, Italy, p. 1.

[35] Dellacorte, C. and Moore, L. E., 2014, "The Effect of Indenter Ball Radius on the Static Load Capacity of the Superelastic 60NiTi for Rolling Element Bearings," *69th Society of Tribologists and Lubrication Engineers (STLE) Annual Meeting and Exhibition*, Lake Buena Vista, FL, p. 16, NASA/TM-2014-216627.

[36] Della Corte, C., Stanford, M. K., and Jett, T. R., 2015, "Rolling Contact Fatigue of Superelastic Intermetallic Materials (SIM) for Use as Resilient Corrosion Resistant Bearings," Tribology Letters, **57**(3), p. 26, doi: 10.1007/s11249-014-0456-3.

[37] Dellacorte, C., Thomas, F., and Leak, O. A., 2015, "Tribological Evaluation of Candidate Gear Materials Operating Under Light Loads in Highly Humid Conditions," NASA/TM-2015-218896.

[38] Dellacorte, C. and Jefferson, M., 2015, "60NiTi Intermetallic Material Evaluation for Lightweight and Corrosion Resistant Spherical Sliding Bearings for Aerospace Applications, Report on NASA-Kamatics SAA3-1288," *2nd Tribology Frontiers Conference*, p. 20, NASA/TM-2015-218723.

[39] Stanford, M. K., 2015, "Hot Isostatic Pressing of 60-Nitinol," NASA/TM—2015-218884.

[40] Thomas, F., 2015, "The Effect of Various Quenchants on the Hardness and Microstructure of 60-NITINOL," NASA/TM-2015-218463.

[41] Hornbuckle, B. C., Noebe, R. D., and Thompson, G. B., 2015, "Influence of Hf Solute Additions on the Precipitation and Hardenability in Ni-Rich NiTi Alloys," Journal of Alloys and Compounds, **640**, pp. 449–454, doi: 10.1016/j.jallcom.2015.04.002.

[42] Chad Hornbuckle, B., Yu, X. X., Noebe, R. D., Martens, R., Weaver, M. L., and Thompson, G. B., 2015, "Hardening Behavior and Phase Decomposition in Very Ni-Rich Nitinol Alloys," Materials Science and Engineering: A, **639**, pp. 336–344, doi: 10.1016/j.msea.2015.04.079.

[43] DellaCorte, C., Howard, S. A., and Moore, L. E., III, 2016, "Failure Analysis and Recovery of a 50 MM Highly Elastic Intermetallic NiTi Ball Bearing for an ISS Application," *43rd Aerospace Mechanisms Symposium*, p. 16, GRC-E-DAA-TN35928.

[44] Dellacorte, C., 2016, "NiTi Alloys for Tribological Applications: The Role of In-Situ Nanotechnology," .

[45] Stanford, M. K., 2016, "Hardness and Microstructure of Binary and Ternary Nitinol Compounds," NASA/TM-2016-218946,.

[46] Stanford, M. K., 2016, "Preliminary Investigation of Surface Treatments to Enhance the Wear Resistance of 60-Nitinol," NASA/TM-2016-219121.

[47] Dellacorte, C., Howard, S. A., Thomas, F., and Stanford, M. K., 2017, "Microstructural and Material Quality Effects on Rolling Contact Fatigue of Highly Elastic Intermetallic NiTi Ball Bearings," NASA/TM-2017-219466.

[48] Stanford, M. K., 2017, "Hardness and Second Phase Percentage of Ni-Ti-Hf Compounds After Heat Treatment at 700C," .

[49] Stanford, M. K., 2018, "Friction and Wear of Unlubricated NiTiHf with Nitriding Surface Treatments," NASA/TM-2018-219740.

[50] Stanford, M. K., 2018, "Fractographic Analysis of 60-Nitinol Bearing Races," NASA/TM-2018-219905.

[51] Stanford, M. K., 2019, "Dry Sliding of Nitrided NiTiHf," Tribology Transactions, pp. 1–9, doi: 10.1080/10402004.2018.1562137.

[52] Oberle, T. L., 1951, "Wear of Metals," Journal of Metals.

[53] Patil, D., Marinack, M. C., DellaCorte, C., and Higgs, C. F., 2017, "Experimental Investigations of the Superelastic Impact Performance of Nitinol 60," Tribology Transactions, **60**(4), pp. 615–620, doi: 10.1080/10402004.2016.1191694.

[54] Khanlari, K., Ramezani, M., and Kelly, P., 2018, "60NiTi: A Review of Recent Research Findings, Potential for Structural and Mechanical Applications, and Areas of Continued Investigations," Transactions of the Indian Institute of Metals, **71**(4), pp. 781–799, doi: 10.1007/s12666-017-1224-5.

[55] Khanlari, K., Ramezani, M., Kelly, P., Cao, P., and Neitzert, T., 2018, "Comparison of the Reciprocating Sliding Wear of 58Ni39Ti-3Hf Alloy and Baseline 60NiTi," Wear, **408-409**, pp. 120–130, doi: 10.1016/J.WEAR.2018.05.011.

[56] Roberts, R. W. and Owens, R. S., 1963, "Titanium Lubrication," Nature, **200**(4904), pp. 357–358, doi: 10.1038/200357a0.

[57] Khanlari, K., Ramezani, M., Kelly, P., Cao, P., and Neitzert, T., 2018, "An Investigation on Reasons Causing Inferiority in Unlubricated Sliding Wear Performance of 60NiTi as Compared to 440C Steel," Tribology Transactions, pp. 1–14, doi: 10.1080/10402004.2018.1516326.

[58] Khanlari, K., Ramezani, M., Kelly, P., Cao, P., and Neitzert, T., 2018, "Reciprocating Sliding Wear Behavior of 60NiTi As Compared to 440C Steel under Lubricated and Unlubricated Conditions," Tribology Transactions, **61**(6), pp. 991–1002, doi: 10.1080/10402004.2018.1460434.

[59] Miller, P. D. and Holladay, J. W., 1958, "Friction and Wear Properties of Titanium," Wear, **2**(2), pp. 133–140, doi: 10.1016/0043-1648(58)90428-9.

[60] Miller, C., Choudhury, D., and Zou, M., 2019, "The Effects of Surface Roughness on the Durability of Polydopamine/PTFE Solid Lubricant Coatings on NiTiNOL 60," Tribology Transactions, **0**(ja), pp. 1–10, doi: 10.1080/10402004.2019.1641645.

[61] Budinski, K. G., 1991, "Tribological Properties of Titanium Alloys," Wear, **151**(2), pp. 203–217, doi: 10.1016/0043-1648(91)90249-T.

[62] Zhang, R., Mankoci, S., Walters, N., Gao, H., Zhang, H., Hou, X., Qin, H., Ren, Z., Zhou, X., Doll, G. L., Martini, A., Sahai, N., Dong, Y., and Ye, C., 2019, "Effects of Laser Shock Peening on the Corrosion Behavior and Biocompatibility of a Nickel–Titanium Alloy," Journal of Biomedical Materials Research Part B: Applied Biomaterials, **107**(6), pp. 1854–1863, doi: 10.1002/jbm.b.34278.

[63] Hou, X., Mankoci, S., Walters, N., Gao, H., Zhang, R., Li, S., Qin, H., Ren, Z., Doll, G. L., Cong, H., Martini, A., Vasudevan, V. K., Zhou, X., Sahai, N., Dong, Y., and Ye, C., 2018, "Hierarchical Structures on Nickel-Titanium Fabricated by Ultrasonic Nanocrystal Surface Modification," Materials Science and Engineering: C, **93**, pp. 12–20, doi: 10.1016/j.msec.2018.07.032.

[64] ZENG, Q.-f., ZHAO, X.-m., DONG, G.-n., and WU, H.-x., 2012, "Lubrication Properties of Nitinol 60 Alloy Used as High-Speed Rolling Bearing and Numerical Simulation of Flow Pattern of Oil-Air Lubrication," Transactions of Nonferrous Metals Society of China, **22**(10), pp. 2431–2438, doi: 10.1016/S1003-6326(11)61481-7.

[65] Zeng, Q. and Dong, G., 2013, "Influence of Load and Sliding Speed on Super-Low Friction of Nitinol 60 Alloy under Castor Oil Lubrication," Tribology Letters, **52**(1), pp. 47–55, doi: 10.1007/s11249-013-0191-1.

[66] Zeng, Q. and Dong, G.-n., 2014, "Superlubricity Behaviors of Nitinol 60 Alloy under Oil Lubrication," Transactions of Nonferrous Metals Society of China, **24**(2), pp. 354–359, doi: 10.1016/S1003-6326(14)63068-5.

[67] Zeng, Q., Dong, G., and Martin, J. M., 2016, "Green Superlubricity of Nitinol 60 Alloy against Steel in Presence of Castor Oil," Scientific Reports, **6**(1), p. 29992, doi: 10.1038/srep29992.

[68] Yan, C., Zeng, Q., Hao, Y., Xu, Y., and Zhou, M., 2019, "Friction-Induced Hardening Behaviors and Tribological Properties of 60NiTi Alloy Lubricated by Lithium Grease Containing Nano-BN and MoS2," Tribology Transactions, **0**(0), pp. 1–9, doi: 10.1080/10402004.2019.1619889.

[69] Tylczak, J. H., Hawk, J. A., and Wilson, R. D., 1999, "A Comparison of Laboratory Abrasion and Field Wear Results," Wear, **225-229**, pp. 1059–1069, doi: 10.1016/S0043-1648(99)00043-5.

[70] Bhushan, B., 2000, *Modern Tribology Handbook, Two Volume Set*, CRC Press, doi: 10.1201/9780849377877.

[71] Asadauskas, S., Perez, J. M., and Duda, J. L., 1997, "Lubrication properties of castor oil - Potential basestock for biodegradable lubricants," Lubrication Engineering, **53**, pp. 35–40.

[72] Bongfa, B., Atabor, P. A., Barnabas, A., and Adeoti, M. O., 2015, "Comparison of Lubricant Properties of Castor Oil and Commercial Engine Oil," Jurnal Tribologi, **5**, pp. 1–11.

[73] Mark T. Stahl and H. Philip Stahl, 2013, "Incorporating Skew into RMS Surface Roughness Probability Distributions," *SPIE Optical Engineering + Applications* (Vol. 8838), San Diego, California, p. 14, doi: 10.1117/12.2024883.

[74] NASA, 2016, "Design and Development Requirements for Mechanisms," Technical Standard NASA-STD-5017, NASA.

[75] Wilson, A. R., 1979, "The Relative Thickness of Grease and Oil Films in Rolling Bearings," Proceedings of the Institution of Mechanical Engineers, **193**(1), pp. 185–192, doi: 10.1243/PIME_PROC_1979_193_019_02.

[76] Lugt, P. M., 2009, "A Review on Grease Lubrication in Rolling Bearings," Tribology Transactions, **52**(4), pp. 470–480, doi: 10.1080/10402000802687940.

[77] Buckley, D. H. and Johnson, R. L., 1966, "Friction, Wear, and Adhesion Characteristics of Titanium-Aluminum Alloys in Vacuum," NASA-TN-D-3235.

[78] Roberts, R. W. and Owens, R. S., 1963, "Boundary Lubrication of Titanium-Titanium and Tttanium-Steel," Wear, **6**(6), pp. 444–456, doi: 10.1016/0043-1648(63)90280-1.

[79] Richard W Roberts, R. S. O., 1966, "Lubricants Containing Charge Transfer Complexes of Iodine and Aromatic Compounds," U.S. Patent 3228880A.

[80] Boehm, J., 1970, "Amine-Stabilized Iodine-Containing Lubricants," U.S. Patent 3499839A.